FLUX MOTION IN SUPERCONDUCTORS

H. VAN BEELEN

INSTITUUT-LORENTZ
voor theoretische natuurkunde
Nieuwsteeg 18-Leiden-Nederland

FLUX MOTION IN SUPERCONDUCTORS

FLUX MOTION IN SUPERCONDUCTORS

PROEFSCHRIFT

TER VERKRIJGING VAN DE GRAAD VAN DOCTOR IN DE WISKUNDE EN NATUURWETENSCHAPPEN AAN DE RIJKSUNIVERSITEIT TE LEIDEN OP GEZAG VAN DE RECTOR MAGNIFICUS DR P. MUNTENDAM, HOOGLERAAR IN DE FACULTEIT DER GENEESKUNDE, TEN OVERSTAAN VAN EEN COMMISSIE UIT DE SENAAT TE VERDEDIGEN OP MAANDAG 23 OKTOBER 1967 TE 16 UUR.

DOOR

HUGO VAN BEELEN

GEBOREN TE 'S-GRAVENHAGE IN 1934

1967

KONINKLIJKE DRUKKERIJ VAN DE GARDE N.V.

ZALTBOMMEL

Promotor: PROF. DR. K. W. TACONIS

Dit proefschrift is bewerkt mede onder toezicht van Dr. R. de Bruyn Ouboter

Aan mijn ouders

Aan mijn vrouw

STELLINGEN

I

Van het door Voigt berekende potentiaalverschil dat optreedt over de pompbrug van de „Leidse fluxpomp" tijdens de beweging van de flux door de brug, geeft slechts de term welke het gevolg is van de al in het circuit aanwezige stroom aanleiding tot een vermindering van de pompsnelheid.

H. Voigt, Z. Naturforsch. **21a** (1966) 510.
Hoofdstuk I van dit proefschrift.

II

Doordat bij het lopen van vortices in type II supergeleiders irreversibele warmte wordt ontwikkeld, is het moeilijk uit soortelijke warmte metingen conclusies te trekken over de aard van de overgang van de volledig supergeleidende toestand naar de gemengde toestand.

III

Bij de ontwikkeling van materialen voor de bouw van krachtige supergeleidende magneten wordt te weinig rekening gehouden met het bestaan van fluxpompen.

Hoofdstuk I van dit proefschrift.

IV

Het door Gifford en Longsworth aangegeven principe van „surface heat pumping" kan ook bij lagere temperaturen worden toegepast.

W. E. Gifford en R. C. Longsworth, 1964: „International Advances in Cryogenic Engineering", 10 (Section M–W), 69, Plenum Press, New York.

V

Het geeft minder inzicht de eerste orde correctie op de snelheidsdistribu-

tiefunctie van een éénatomig gas in niet uniforme toestand uit te drukken in de gradiënt van de macroscopische grootheden dan in de flux.

S. Chapman en T. G. Cowling, „The Mathematical theory of non-uniform gases" Cambridge University Press, 1960.

VI

De nauwkeurigheid van de door Hess en Fairbank verrichte metingen van het impulsmoment van superfluïde helium is op te voeren door een rotor met meerdere cylindrische holtes te nemen.

G. B. Hess, Proefschrift 1967.
G. B. Hess en W. M. Fairbank, Phys. Rev. Letters **19** (1967) 216.

VII

De wederkerige acoustische impedantie van twee geluidselementen in een oneindig plat vlak kan eenvoudig worden berekend voor het geval de diameter van de geluidsbron klein is ten opzichte van de golflengte van het geluid. Uit een dergelijke berekening volgt dat het resultaat van Pritchard het verkeerde teken heeft.

R. L. Pritchard, JASA **32** (1960) 730.

VIII

De opmerking van Gersdorf, Muller en Roeland dat bij een axiaalsymmetrische belasting van een axiaalsymmetrisch lichaam alle schuifspanningen nul zijn is onjuist.

R. Gersdorf, F. A. Muller en L. W. Roeland, Rev. Scient. Instr. **36** (1965) 1100.

IX

De door French, Lowell en Mendelssohn in niobium preparaten met 5 at.% molybdenium gevonden sterke stroomafhankelijkheid van de soortelijke weerstand in de supergeleidende gemengde toestand, kan, hoewel deze preparaten een vrijwel reversibele magnetisatiekromme vertonen, goed worden verklaard uit de aanwezigheid van sterke „pinning centra".

R. A. French, J. Lowell en K. Mendelssohn, Cryog. **7** (1967) 83.
Hoofdstuk IV, § 3b, van dit proefschrift.

X

Het door Dornberger-Schiff en Leciejewicz en door Berger, Friedberg en Schriempf opgegeven aantal kristalwatermoleculen in het als kopernitraat-trihydraat bekend staande zout, is aan bedenkingen onderhevig.

K. Dornberger-Schiff en J. Leciejewiz, Acta Cryst. **11** (1958) 825.
L. Berger, S. A. Friedberg en J. T. Schriempf, Phys. Rev. **132** (1963) 1057.

XI

Om te komen tot betere warmteuitwisselaars in koelmachines die van de mengwarmte van ^3He–^4He mengsels gebruik maken, is het van belang het anomale gedrag van de overgangs-warmte weerstand van cerium-magnesium nitraat in vloeibaar ^3He nader te bestuderen. -

W. R. Abel, A. C. Anderson, W. C. Black en J. C. Wheatley, Phys. Rev. Letters **16** (1966) 273.

XII

De nauwkeurige overeenstemming die Segal meent te hebben gevonden tussen de berekende en gemeten initiële veldverandering in een pulsmagneet kan slechts voor de initiële stroomverandering bewezen worden geacht.

G. P. Segal, Rev. Scient. Instr. **37** (1966) 1367.

CONTENTS

INTRODUCTION

In the thesis some aspects of the problems encountered when flux tubes move through a superconducting sheet are discussed. One has to distinguish between the motion of a large flux bundle and the motion of a mixed-state pattern.

Large flux bundles are created with an external magnetic field higher than the critical field of the superconducting sheet. The flux bundle intersects the sheet through an area of normal material. A mixed-state pattern can be obtained by applying a magnetic field, with a strength lower than the upper critical field, perpendicularly to a sheet of type II superconducting material. In this case the magnetic flux penetrates the specimen through small flux tubes, the so called Abrikosov vortices; each tube containing a single flux quantum Φ_0.

The motion of the large flux bundles, which can be achieved by moving the external magnet, only gives rise to a small electric potential difference across the sheet, since the local region of normal material is surrounded by a completely superconducting region. Currents, induced by the motion are thus short-circuited. This feature can be used for the construction of flux pumps, devices with which magnetic flux can be brought into closed superconducting circuits (chapter I). The motion of the mixed-state patterns can be generated, for instance, by the motion of an external magnet (chapter II) or by driving a transport current through the mixed-state area. The problems which arise in these cases can be summarised in two main questions:

1) what is the equation of motion for the mixed-state pattern?

2) if the motion is known, what are the voltages observed due to this motion?

In order to obtain an answer to the second question, one could try to impose a known velocity on a mixed-state pattern and measure the generated voltages. It will be shown in chapter II that one can only do so in the case

of a local mixed-state region, surrounded by flux-free superconducting material. In this situation the vortices will be dragged along with the magnetic induction, and with a voltmeter one observes a voltage equal to the total flux transport *across the voltmeter leads* into the voltmeter circuit. If a uniform mixed-state pattern moves under the influence of a transport current there is no net flux transport connected with this motion. It will be shown (chapter II and III) that now an observable potential difference is built up across the sample equal to the flux transport which would be there if the magnetic induction, $B = N\Phi_0$, were moving with the vortices.

Once the answer to question 2 is known, one could find the answer to question 1 experimentally, if the effects due to flux pinning would not complicate things. Theoretically one obtains the answer to question 1, e.g. by starting from the fact that the force, exerted by an external magnetic field on a conductor carrying a current is always equal to the Lorentz force, independent of the current- and field-distribution within the conductor. It will be shown (chapter III) that a mixed-state pattern driven by a transport current obtains a velocity component parallel as well as transverse to the transport current. It is thus clear that a pinning-free type II superconductor in a perpendicularly applied magnetic field, exhibits resistivity as well as a Hall effect. As different theories predict different magnitudes of these effects, it is of interest to decide from experiment upon this question. However, in chapter IV it will be shown how flux pinning, i.e. the vortices cannot move freely through the material, complicates the interpretation of the experimental results.

CHAPTER I

FLUX PUMPS AND SUPERCONDUCTING SOLENOIDS

Synopsis

A review is given of the various types of flux pumps and current generators which have been developed so far in several laboratories. Experiments carried out with wire- and foil-solenoids, fed by the flux pump developed in the Kamerlingh Onnes Laboratory, are discussed. It is shown that 50 kOe, many-strand wire solenoids with a central core diameter of the order of a few centimeters, can at the present time be fed with this flux pump in a competitive way compared to feeding them with the ordinary current supplies from outside the liquid helium dewar. Attention is paid to the unavoidable heat dissipation in this type of pump. The experiments with foil-solenoids show a disappointingly low current carrying capacity of the Nb–Zr foil in comparison with that of wires of the same type of material. An explanation of the results on the basis of the critical-state theory is proposed. From the pumping characteristics it is shown that starting off at a certain critical field, a gradual change of selfinduction of the coil occurs.

1. *Introduction.* Since the discovery of superconductivity by Kamerlingh Onnes in 1911[1]), attempts have been made to construct superconducting magnets. It was soon discovered, that small magnetic fields, usually of the order of a few hundred oersted, are sufficient to destroy superconductivity[2]), and it was not until 1931 that new hope was raised by the discovery of new superconductive materials[3]) with more promising magnetic properties. These were alloys of the superconducting elements with themselves or even with elements not known to be superconducting which showed no sign of restoration of resistance in magnetic fields up to several kilooersteds. For instance, the measurements of De Haas and Voogd[3]) on the eutectic Pb–Bi showed at 4.2°K the first trace of resistance only in a field of nearly 16 kOe. However, the attempts of Keesom[4]) and of Rjabinin and Schubnikov[5]) to construct magnets from this material, meant to produce a field of some kilooersteds, turned out to be a great disappointment. As we know now, the Lorentz force on the current reduces the current carrying capacity of these soft materials so far below the expected Silsbee value that only current densities of some hundred A/cm^2 are

left in these fields. For example with a current density of 400 A/cm^2 a magnet with an outer diameter and a length of the order of 1 meter would be required to produce a field of 15000 Oe in a 1 cm diameter core. For the production of fields in the 10–100 kOe range with air-core magnets of reasonable size, current densities of at least 3×10^4 A/cm^2 are required.

Despite some early successes with iron-core Nb magnets (25 kOe) of Autler[6]) and with air-core Nb wire magnets of Yntema (1955)[7]) and Autler (1960)[8]) (in which fields of more than 8 kOe were achieved) and with a Mo_3Re solenoid by Kunzler *e.a.* (1961)[9]), it was only with the discovery of the high current carrying capacities of the superconducting materials Nb–25 at.% Zr[10]) and Nb_3Sn[11]) that all requirements for the construction of high-field superconducting magnets seemed to be fulfilled. With current carrying capacities of 5×10^4 A/cm^2 in fields as high as 60 kOe for Nb–Zr[12]) and of 2×10^5 A/cm^2 in fields up to 88 kOe for Nb_3Sn[13]) it seemed that nothing would be able to stop their rapid development.

The hardness of both materials and the extreme brittleness of the Nb_3Sn, however, caused great difficulties in the production of long lengths of uniform quality wire, required for the construction of solenoids. New techniques had to be developed for the manufacturing of wires and one has now reached the stage, that fairly long lengths of Nb–Zr wire can be produced. In the case of Nb_3Sn a technique is often used in which a Nb tube, filled with Nb and Sn powder is drawn into wire. This wire is wound into a solenoid and sintered afterwards to produce the Nb_3Sn[13]). In this way solenoids which produce fields up to 68 kOe have been constructed from Nb–Zr wire[14]) while with Nb_3Sn a 100 kOe field has been reached[15]). For the latter a slightly different technique was used in which a tin-clad niobium wire, insulated with a ceramic material was wound into a solenoid and sintered afterwards. More recently another alloy, Nb–25% Ti similar in metallurgical and superconducting properties to Nb–25% Zr, has been used for the construction of solenoids which also produce fields up to 100 kOe[16]). Also a 107 kOe magnet was reported, wound from a prefabricated Nb_3Sn ribbon[17]).

Several unexpected difficulties turned up in the behaviour of the wires being wound into solenoids. Some are:

a) *Training effects* in Nb–Zr coils, *i.e.*, the occurrence of critical currents, far below the maximum critical current, on which the coil suddenly turns normal. By reducing the rate of increase of current through the coil those critical points can be passed and the coil can reach the maximum current.

b) *Flux jumps* in Nb–Ti solenoïds, which occur mainly in the lower field region up to about 20 kOe.

c) *Current degradation*, the lower critical current of inductively wound Nb–Zr wire, in comparison with the short-sample value in the same field.

d) Damage done by *inductive voltages*, occurring when the coil suddenly turns normal.

Although at present these effects are not always well understood, considerable progress has been made to reduce their influence. Special devices for current supply have been developed to avoid the training effects. Copper or silver plating of the wires increases their current carrying capacities and decreases the inductive voltages. Flux jumps in Nb–Ti solenoids are avoided by placing these coils in an outer field of over 20 kOe, which is produced for instance by a surrounding Nb–Zr solenoid[17]).

With the development of these high current carrying capacity materials, the need for high current generators operating inside the liquid helium bath, is obvious. The use of Nb_3Sn wire as thin as 0.25 mm in diameter already makes currents of the order of 100 A necessary, while the use of thicker wires or foils – the latter to gain considerably in the space factor of the coil – readily requires currents of the order of 1000 A. Because of the heat dissipation in the supply leads such large currents cannot possibly be fed into a helium dewar from the outside.

This chapter is mainly concerned with the development of these types of current generators, the so-called flux pumps, and with their applications for the current supply of high field superconducting magnets.

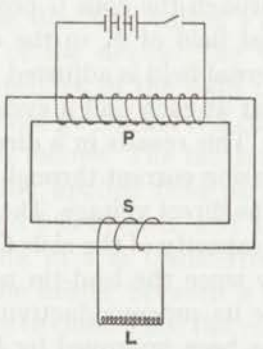

Fig. 1. The Mendelssohn transformer.

2. *Review of various current generators and flux pumps. a.* The Mendelssohn transformer. The first superconducting generator was constructed as early as in 1933 by Mendelssohn[18]). A direct current transformer with superconducting secondary is used (fig. 1). A current is fed from outside the helium dewar into the primary winding of the transformer. The superconducting secondary circuit consists of a secondary with a few turns of large radius and a solenoid with many narrow turns for producing the field. The secondary circuit is cooled down below its critical temperature with the primary current being kept constant. If the primary current is now switched

off, a persistent secondary current builds up in order to keep the total flux linked in the superconducting circuit constant. This transformer is not practical to feed large volume-or high field-magnets since the required size of the transformer becomes prohibitive.

b. The Olsen device. A device without the latter difficulty has been developed by Olsen[19]). A low alternating current is fed into the many turns primary of a superconducting transformer. The high secondary current is rectified by leading it through the two small lead-tin coils *C*. These coils

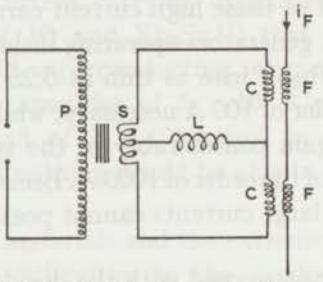

Fig. 2. The Olsen device.

are placed in the magnetic field of the coils *F* in such a way that, during each half a cycle, the current through the coils *C* produces in one of the coils a field parallel to the external field of *F*, in the other coil the fields are of opposite direction. The external field is adjusted just below the critical field value of the lead-tin, so that at each half a cycle the current in one of the coils *C* is mainly quenched. This results in a direct voltage over the coil *L*, which gives rise to an increasing current through *L* with a slope $\bar{V}/L$, where $\bar{V}$ is the averaged value of the direct voltage. The limitation of the current is set by the current carrying capacity of the coils *C*. The switching of the coils has to be timed accurately since the lead-tin needs a finite time interval during each cycle to restore its superconductivity.

The rectifying system has been improved by Buchhold[19]). The coils *C* are replaced by high-current switches made of Nb foil. Each switch is operated by a coil which can give a strong enough field, to restore sufficient resistance in the niobium. The switching is performed by a "saturable reactor" which is placed in the circuit. It operates the current supply of the coils in a way such that the current growth in the Nb foil is postponed during the retardation time. This prevents the Nb from being heated above its critical temperature by this current. It was reported that this device takes 80 seconds to generate a 280 A persistent current in a 1.8 mH Nb–Zr coil.

c. The flux pumps of *Swartz* and *Rosner* (1962) and *Hildebrandt, Elleman, Whitmore* and *Simpkins*[20]). A schematic diagram of these flux

pumps is given in fig. 3. A solid block of superconducting material contains two cylindrical holes *a* and *b*, which are joined by a narrow slot. The block is cooled down under its critical temperature in the presence of an external field applied parallel to the cylinder axis. If the field is switched off, a current is induced in the wall of the cylinders keeping the flux constant. By inserting a superconducting piston in hole *b* (fig. 3A), the field is compressed into the remainder of open area, thus achieving a gain in magnetic field strength in *a* inversely proportional to the ratio of the open areas. By using iron cores

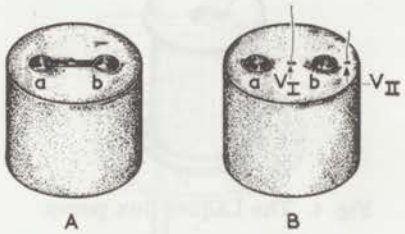

Fig. 3. A. The flux compressor of Swartz and Rosner.
B. The cyclical flux pump of Hildebrandt, Elleman, Whitmore and Simpkins.

in the cylindrical holes during the cooling down, the total flux can be increased, and thus higher fields can be achieved. Another version of this apparatus is sketched in fig. 3*B*. Two valves V_I and V_{II} are added which permit a cyclic operation of the device. The valves are formed by two nichrome heating wires embedded in the walls of the cylinders, which can make the surrounding material go normal if a current is fed into them. The cycle of operation is now as follows. The block is cooled down to 4.2°K in the presence of an externally applied field parallel to cylinders *a* and *b*. The valve V_I between *a* and *b* is opened, and a superconducting piston is inserted in *b*. Thus the flux in *b* is transferred into *a*, through normal material. The current to the heater between *a* and *b* is then interrupted, thereby permitting the valve to close. Then the valve V_{II} between the outside region and *b* is opened, and the piston in *b* is withdrawn. This permits the external field again to be established in *b*. The latter valve is now closed, and then the pump cycle is repeated. With this device fields up to 23.5 kOe in Nb_3Sn blocks are reached while using pumping field strengths of some hundreds of oersteds.

d. The Laquer flux pump[21]). This flux pump operates similarly to the one described under *c* but contains no moving parts and is applicable to feed wire magnets. A sketch is given in fig. 4. With the valve V_2 (a heating wire) opened, the magnetic field of the electromagnet *A* is switched on and subsequently V_2 is closed. On switching off the field of the electromagnet *A*, a flux $\Delta\Phi$ is trapped in the superconducting circuit with self-inductance L_2. After opening of V_1 and closing it again, a fraction of this flux

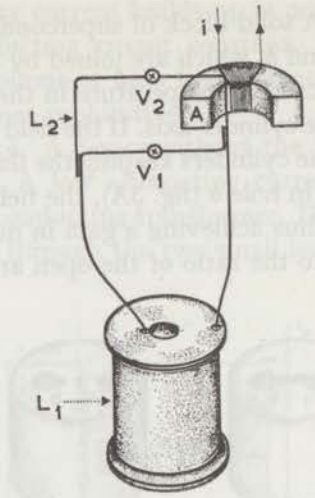

Fig. 4. The Laquer flux pump.

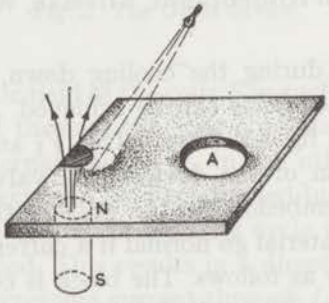

Fig. 5. Flux transport by means of a light beam (Marchand and Volger).

$\Delta\Phi$, $(L_1/(L_1 + L_2))\,\Delta\Phi$ is stored in the selfinductance L_1. The cycle is now permitted to repeat by opening V_2 and switching on the magnetic field of A again. With this procedure a flux Φ in the solenoid L_1 can be built up to a limiting value $\Phi_{max} = (L_1/L_2)\,\Delta\Phi$. Fields up to 5420 Oe are reported in Nb_3Sn with corresponding currents as high as 1070 A.

e. The Marchand and Volger flux pump. An illustrative method of flux transport is described by Marchand and Volger[22]), and is sketched in fig. 5. A region of normal material, created by a permanent magnet on the edge of a thin superconducting lead sheet, is guided towards the hole A in the sheet by means of a small search light beam, of which the heat dissipation on the edge of the normal region is sufficient to make the lead go normal. By moving the light beam towards the hole, the flux carried by the normal region is brought into the hole, and by switching off the light a new amount of flux can be fetched by the bundle.

f. The unipolar dynamo. A very elegant approach was followed by Volger and Admiraal[23]). Fig. 6 shows the device schematically. A thin superconducting disc is cooled down in the presence of a small permanent magnet. Owing to the magnetic field a local region of the disc remains normal if the disc is cooled down below its critical temperature. The permanent magnet is now rotated around the centre of the superconducting disc, to which a superconducting circuit is connected. One connection is made to the centre part of the disc and the other near the edge, as indictated in the

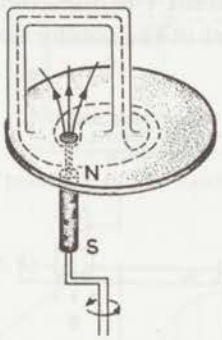

Fig. 6. The unipolar dynamo (Volger and Admiraal).

figure. The moving magnetic field lines of the magnet intersect the closed superconducting circuit in two ways, once in the disc, where a cluster of moving normal regions is formed and once in the rest of the superconducting circuit. In both areas a Lorentz force is exerted on the electrons by the moving field. The resulting electromotive force in the normal regions, however, does not give rise to a current through the circuit*). Since these regions are embedded in superconducting material, only a low-inductive backflow of electricity occurs around the edges of the normal zones. The resulting inductive voltage is small and is neglected in this thesis The current generated by the induced electromotive force in the other part of the circuit, where the moving field is not strong enough to disturb superconductivity, is thus not compensated for.

The overall result can also be understood by means of the integration theorem. The dotted line in fig. 6 represents an integration path chosen in the bulk of the superconducting material. After each revolution of the magnet the flux Φ carried by the normal regions is once more embraced by this integration path if this latter is chosen so that its front moves ahead of the normal regions. Since the flux in a closed superconducting circuit is

*) The interesting problems involved with the motion of flux bundles through a superconducting sheet are discussed in more detail in the next sections of this thesis.

constant, a current must be generated in the circuit which compensates for this flux change. After n revolutions a flux $-n\Phi$ is built up in the superconducting circuit.

It is interesting to give a comparison with some non-superconducting unipolar dynamo's, as are sketched in fig. 7.

Fig. 7*a* shows a sketch of the usual unipolar dynamo, so called by Weber[27]) because one pole of the magnet intersects the plane which has the current path as edge. The so-called Faraday apparatus[24]) is represented in fig. 7*b* and in fig. 7*c* is shown the superconducting unipolar dynamo. All three devices generate a direct current i in the circuit if the magnet is rotated, owing to the fact that one part of the conduction pattern is moving in phase

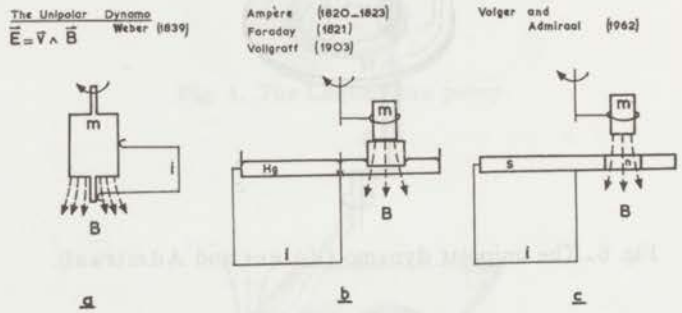

Fig. 7. *a*. The unipolar dynamo (Weber).
b. The Faraday apparatus.
c. The superconducting unipolar dynamo (Volger and Admiraal).

with the rotating magnetic field while the other part is at rest. In Faraday's apparatus the distortion of the conduction path is caused mechanically by the movement of the floating magnet in the mercury liquid. In the Volger-Admiraal apparatus this is achieved magnetically by the creation of a normal region in a thin superconducting disc, which region rotates through the disc in phase with the magnet.

Both devices can also operate as an electromotor. If a direct current is fed into the circuit the magnet rotates backwards. The results obtained with the Volger-Admiraal flux pump look very promising. The pumping speed can be considerably increased by connecting several of these devices in series.

3. *The Leiden flux pump. a.* Principle. A sketch of the principle on which the Leiden flux pump[25])[26])[27]) is based is given in fig. 8. A superconducting circuit L is connected to a thin superconducting sheet. A flux is brought into the closed circuit by moving the pole area of a small U-frame electromagnet from position P to position Q with the field switched on,

and the direction of the magnetic field being perpendicular to the sheet. In this way a region of normal material is created in the superconducting sheet when the magnet passes the edge, since no shielding currents can prevent this here. This region moves with the magnet towards the interior of the circuit. However, no current is generated to compensate for the flux which is thus brought into the circuit, since the electromotive force, which originates in the normal region – arising from the Lorentz force which is exerted on the electrons by the moving field (fig. 9) [28] – results mainly in an induction-free

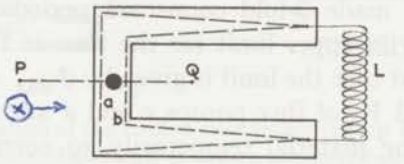

Fig. 8. The principle of the Leiden flux pump.

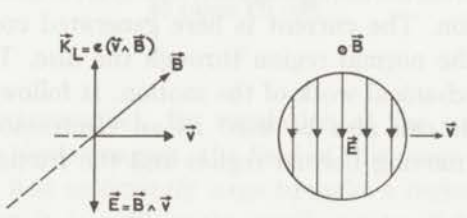

Fig. 9. The electric field strength in the region of moving normal material.

backflow of electricity around the edges of the normal region. That no current is generated in the circuit can also be seen with the conservation law of flux. The two dotted lines in fig. 8 represent two integration paths *a* and *b*, which are chosen in the bulk of the superconductor and which close in the circuit *L*. During the movement of the normal region over the sheet, no change of the flux embraced by either of them is allowed as long as no part of them becomes normal. Thus, when the normal region moves from the edge and passes integration path *a*, no current can be generated in the circuit due to the conservation of flux embraced by *b*. Further, after the flux-carrying normal region has passed *a* no changes in flux are allowed because of flux conservation in *a*. This is all true provided that all flux lines close in the yoke of the electromagnet and thus intersect the circuit only in the normal region. Intersection of unavoidable stray flux with the circuit gives rise to alternating current components.

If, from position *Q* (fig. 8) the field of the electromagnet is now brought out of the circuit without disturbing superconductivity or if the field is switched off or reversed in *Q*, a current is generated in the circuit to obey the conservation law of flux. If the field is switched off, the magnet can

freely be moved back to position P, and the cycle can be repeated. On bringing back the magnet to P with opposite field, however, a normal region is again created. Thus twice the amount of flux carried by the magnet is brought into the circuit at every cycle. In both ways a flux can be built up which is limited only by the superconducting properties of the circuit*).

By carrying out the pumping cycle with opposite pumping field the circuit can be emptied.

The resemblance with the flux pumps described under *c* and *d* should be noticed. The Leiden flux pump, however, has basically a 2-fold connected circuit which is only made 3-fold connected periodically by the normal region. Thus there is no upper limit for the flux as for instance exists in Laquer's pump; in that case the limit is given by $\Phi_{max} = (L_1/L_2)\,\Delta\Phi$*). The electric valves V_1 and V_2 of flux pumps *c* and *d* are used to make a part of the superconducting material temporarily go normal. This function is taken over here by the magnetic field itself.

The Volger-Admiraal current generator, however, is based on the principle of unipolar induction. The current is here generated continuously during the movement of the normal region through the disc. The field energy is supplied by the mechanical work of the motion. It follows that the Volger-Admiraal apparatus can also be used as an electromotor, if dissipative phenomena in the moving normal region and the friction in the bearings are small enough.

In the Leiden flux pump the direct current is generated discontinuously when the field of the electromagnet is either switched off or reversed (or when the flux is brought out of the circuit without disturbing superconductivity). The principle of the Leiden flux pump can also be used for an electromotor.

b. Some modifications of the Leiden flux pump. The first modification (I) of the Leiden flux pump is shown in fig. 10**). The pumping circuit consists here of an indium and a lead sheet, both U-shaped, which at one side are soldered to each other. Both are fixed on a circular glass substrate. The coil is connected to the open ends of the indium and lead strips (fig. 10*b*). Instead of moving the magnet back and forth over the indium with the field being reversed at every turning point, in this device the whole disc is now slowly rotated around its central axis between the

*) Recently it has been shown by Voigt[33]) that a small opposing voltage, proportional to the current through the circuit, is generated during the motion of the normal region through the sheet, thus providing for a limiting maximum current in the circuit. Voigt's calculations are supported by the measurements of Weber[34]) and also by the curve given in fig. 11. However, these results can also be explained from the changes of the field of the iron magnet due to the current in the circuit.

) A similar device is reported by R. W. Boom, Bull. amer. phys. Soc. **8 (1963) 361.

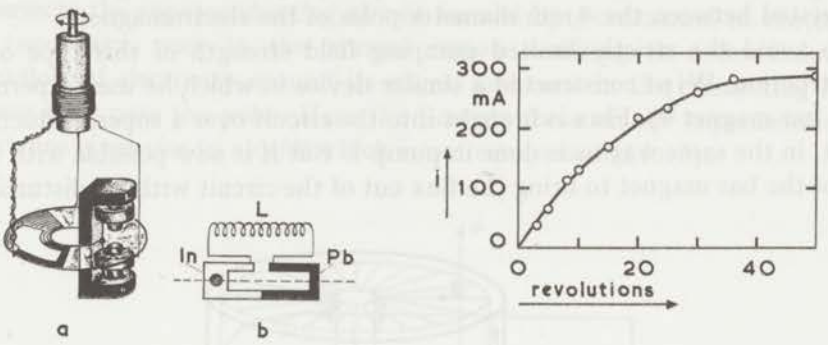

Fig. 10. The first realisation of the Leiden flux pump (pump I). In fig. 10*b* the superconducting circuit is drawn schematically.

Fig. 11. A typical pumping characteristic as obtained with pump I connected to a 40 turns Pb coil.

poles of a tiny electromagnet. By regulation of the current through the Nb wire coil of the electromagnet, the field of this magnet can be adjusted in such a way that it is sufficiently large to make a region in the indium go normal. In addition it is sufficiently small not to disturb the superconductivity of the lead when it passes through the pole gap of the magnet. The circuit L consisting of a coil is rotated with the disc. A pick-up coil is wound around this coil and is connected to a ballistic galvanometer to measure the changes of field in L.

This construction is in no way applicable for the current supply of big superconducting magnets, since the strictly limited pumping field strength leads to impractically long pumping times. However, it demonstrates the features of this type of flux pumping. The pick-up device measures instantaneously every flux change in L. The total current in the circuit is measured by increasing the field of the electromagnet sufficiently to disturb superconductivity over the whole width of the small lead strip when it passes the magnet. This makes the current in the circuit fall rapidly back to zero. The alternating current components caused by a sudden change of the field pattern of the electromagnet by the diamagnetism of the superconducting strips, were nicely observed and occurred every time one of the edges of the foils passed the magnet. This effect reduces the effective pumping field strength.

An example of the pumping characteristic is given in fig. 11, where the total current through a small 40 turns Pb wire coil is plotted as a function of the number of revolutions. The slope at the origin of this pumping

characteristic corresponds roughly to a pumping flux of 10 gauss cm^2 per revolution, which implies an effective pumping field strength of about 80 oersted between the 4 mm diameter poles of the electromagnet.

To avoid the strictly limited pumping field strength of this type of a construction, Wipf constructed a similar device in which he used a permanent bar magnet [29]). Flux is brought into the circuit over a superconducting sheet, in the same way as is done in pump I. But it is now possible with the use of the bar magnet to bring the flux out of the circuit without disturbing

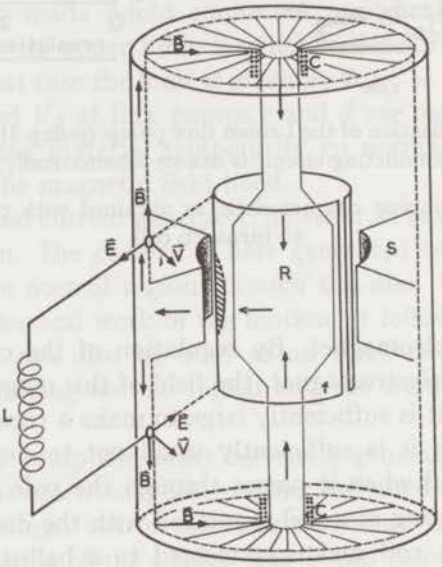

Fig. 12. A sketch of the 3-phase a.c. current flux pump from Van Houwelingen, Admiraal and Van Suchtelen.

superconductivity by placing the other parts of the circuit far away from the pole of the magnet. In this way the pumping field strength is not limited. By using several of these systems in series the pumping speed can still be increased considerably.

The same author also reported a device, in which the moving permanent magnet is replaced by a row of electromagnets. These are fed with a 3-phase alternating current superimposed on a direct current, thus giving rise to a moving flux bundle [29]). Another device without moving parts was reported by Van Houwelingen, Admiraal and Van Suchtelen [30]). A sketch of the principle is given in fig. 12. A rotating field is produced by a 3-phase alternating current between the poles S in the figure; this field is superimposed on a constant field generated by the two coils C. A superconducting foil f is wound around the soft-iron central axis R. There where the direction of the *a.c.* field and *d.c.* field are parallel, a normal region is

created in the foil which is made possible by the gap in the foil. The region moves through the foil around the central axis. Again the moving flux intersects the superconducting circuit formed by f connected to the coil L in two ways, once in the normal region resulting in a low-inductive backflow of electricity around its edges, and once in the connecting leads where they pass the yoke. Here the Lorentz force on the superconductive electrons gives rise to a di/dt which is not compensated for*).

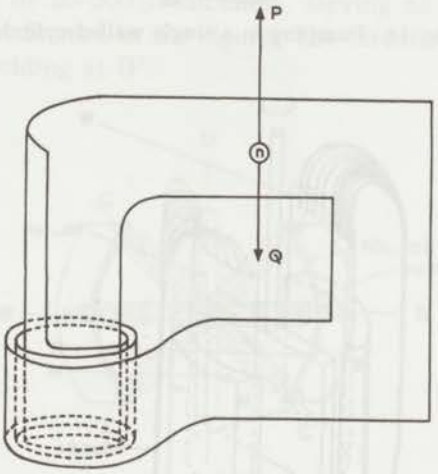

Fig. 13. Schematic drawing of the pumping bridge connected to a foil solenoid as is used in pump II.

A higher pumping speed is obtained in the second version of the Leiden flux pump (II)[25–27]. This pump is operated in the way depicted in fig. 8. The pole area of a tiny electromagnet is moved up and down between P and Q over the superconducting foil which forms the pumping bridge, the field being reversed at every turning point (fig. 13). Pumping speeds of 4×10^3 gauss cm^2 per stroke are achieved, which correspond to an effective pumping field of 16000 oersted between the poles of the electromagnet. With this device a pumping frequency of up to 50 strokes per minute can be achieved leading to a speed of 2×10^5 gauss cm^2 per minute. This speed is sufficiently high to build up high fields in reasonably short times in low-inductance solenoids, wound from foils or thick wires. For instance, it would take less than 10 minutes to build up a 20 kOe field in a 50 turns foil magnet of 1.5 cm inner diameter, made from appropriate superconducting material.

An interesting modification of pump II is sketched in fig. 14, and is applicable for flux pumping in single walled superconducting cylinders.

*) A fluxpump without moving parts was also reported by B. S. Blaisse, O. Kickert, G. J. C. Bots and L. A. Sipman, Phys. Lett. **14** (1965) 5.

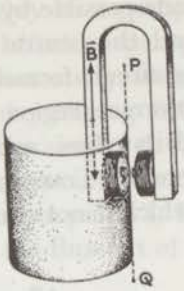

Fig. 14. Pumping in a single walled cylinder.

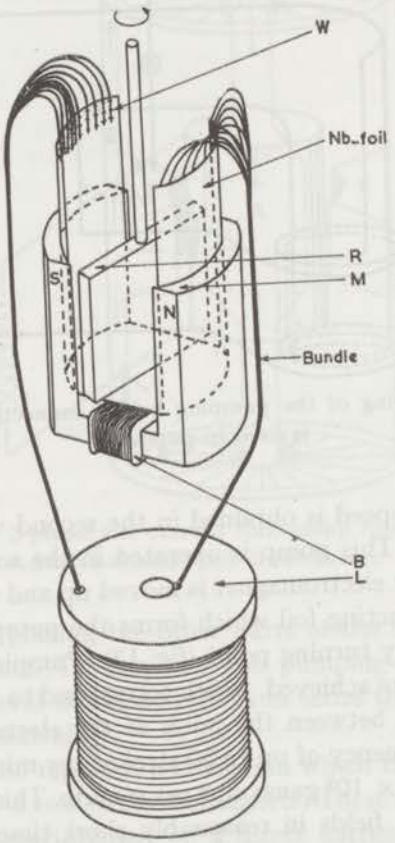

Fig. 15. The rotating Leiden flux pump III.

Flux is pumped into the cylinder by moving the electromagnet up and down between positions Q and P, the field in the yoke embraced by the circuit being reversed in both outer positions. This occurs due to the formation of a normal region in the wall of the superconducting cylinder.

A still higher pumping speed is achieved in another, more effective

realisation of the Leiden flux pump (III)[31]), which is shown connected to a coil L in fig. 15. The translational motion of the field is here modified in a rotational one, thus allowing a larger number of pumping cycles per minute. At the same time the pole area of the electromagnet is increased. A soft-iron rotor R, 6 mm wide and 18 mm high, rotates between the poles of the U-shaped yoke of an electromagnet M. The electromagnet is magnetised by feeding a direct current through the 750 turns Nb wire coil B. The rotor fits closely inside M leaving a gap of less than 0.5 mm on both sides. Within this gap a Nb foil of 20–300 μ thickness, serving as pumping bridge, is folded in the way indicated in the figure. The circuit L can be connected to the Nb foil by welding at W.

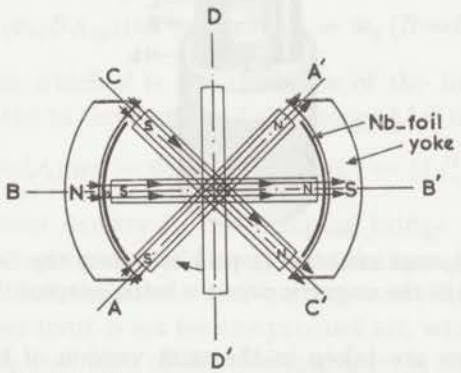

Fig. 16. View from above on pump III.

The view from above of the pumping system is given schematically in fig. 16. During rotation of the rotor from its neutral position $D'D$ the flux guided by the rotor increases. The flux component normal to the loop of the Nb foil pumping bridge links into the circuit and a current is generated to keep the total flux embraced constant. Rotation from AA' to CC' reverses this flux component with respect to the circuit, while normal regions are created in the Nb foil at both ends of the rotor and are transported through the foil. As the normal regions are again embedded in superconducting material, no current change is caused in the circuit to compensate for this flux change, provided that all field lines available intersect the circuit only in the normal regions. Those flux lines which do not fulfill this assumption do here also give rise to alternating current components. The flux guided by the rotor decreases to zero during the rotation from CC' to the neutral position DD' and is built up again in opposite direction with respect to the circuit by moving from DD' to $A'A$. Thus a direct current is generated during rotation from CC' to $A'A$. This builds up a flux in the circuit corresponding to twice the component normal to the circuit of the amount of flux carried by the normal region. Continuous rotation of the rotor in this

way leads per revolution to an increase of flux in the circuit of 4 times the effective pumping flux guided by the rotor.

With this device pumping speeds of 3×10^6 gauss cm^2 per minute are achieved at a revolution speed of 150 cycles per minute. This corresponds to an effective pumping field strength of 5000 Oe in the gap of the electromagnet during the movement of the rotor over the foil. This result shows a gain of a factor 15 in pumping speed compared with the translational pumping system in which we achieved a pumping speed of 2×10^5 gauss cm^2 per minute.

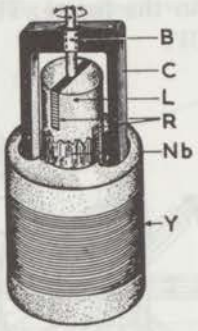

Fig. 17. Pump IV. Special attention is paid to reduce the heat dissipation in this pump, while the magnetic circuit is better adapted than in III.

Some precautions are taken in the next version of this flux pump (IV) in order to prevent the occurrence of extreme heat dissipation and corresponding helium losses due to mechanical causes. The magnetic forces on the rotor (R) during its rotation are reduced by a factor of 2 by constructing the rotor in two sections, perpendicular to each other (fig. 17). Thus friction is reduced in the bearings (B). Friction of the moving rotor with the surrounding He-bath is diminished by embedding the soft iron rotor sections in a "Lorival"*) cylinder (L). Yoke (Y) and rotor are laminated in order to reduce eddy current losses. The magnetic circuit is improved by winding the coil (C) of the magnet directly around the pole area of the yoke, as indicated in fig. 17. With this device pumping speeds up to 10^7 gauss cm^2 per minute are achieved.

c. Heat dissipation in the regions of normal material. With this pump (IV) the helium evaporation can mainly be ascribed to the necessary dissipation by eddy currents in the regions of normal material moving through the bridge foil. The moving magnetic field in the normal zones exerts a Lorentz force on the normal electrons, giving rise to an electric field strength $\boldsymbol{E} = \boldsymbol{v} \times \boldsymbol{B}$. Thus the total heat dissipation per second is given by $\partial W/\partial t = \int\int\int (E^2/\rho_n)\, dV$, where ρ_n is the residual resistance of

*) a cast phenolic resin.

the bridge foil and the integral is taken over the volume of the normal regions. If we roughly assume that $\boldsymbol{B}$ is constant in the normal regions so that $E = vB$ is a constant, the heat dissipation per second becomes

$$\partial W/\partial t = \int\int\int (E^2/\rho_n)\, dV = (v^2B^2/\rho_n)\, V_{spot}.$$

As the rotor passes the foil of width w once, the total heat dissipation equals

$$(v^2B^2/\rho_n)\, V_{spot}\, (w/v) = (vB^2/\rho_n)\, wV_{spot}.$$

This one stroke corresponds to a flux input $\Phi = BA_{spot}$ where A_{spot} is the area of the normal zone. In order to build up a flux Φ_c in the coil L, Φ_c/Φ strokes are necessary. The corresponding heat input into the liquid helium is

$$W = (\Phi_c/BA_{sp})(vB^2/\rho_n)\, wV_{spot} = \Phi_c\, (Bvwd/\rho_n).$$

Here $V_{sp} = A_{sp}d$, in which d is the thickness of the foil. The expression for W can be rewritten in terms of the field energy $\frac{1}{2}Li_c^2$ of the coil:

$$W = \Phi_c\, (Bv/\rho_n)\, wd = \Phi_c i_c (Bv/\rho_n)(wd/i_c) = \tfrac{1}{2}Li_c^2\, 2Bv/\rho_n I_f$$

where I_f is the current density in the pumping bridge. This result shows that in order to build up a given field energy at minimum helium cost, bridge foils with high residual resistance and current carrying capacity are required. Also an upper limit is set for the product vB, which determines the pumping speed if the pole area of the electromagnet is chosen.

That this heat dissipation plays an important role can best be shown with a practical example.

A 260 amperes, 10^{-2} henry NbZr coil, which produces a 26 kOe field in a 19 mm diameter and 10 cm long bore is connected to a pumping bridge of Nb foil. The width of the foil is taken as 2 cm and the thickness 250 micron. By using the rotating pump IV with a pumping field of about 10000 Oe and a linear velocity of 0.2 m/s (which corresponds to a pumping frequency of 3 revolutions per second and a total pumping time of somewhat less than 10 minutes), the calculated heat dissipation corresponds to $W = 260$ joule. The residual resistance of the Nb foil $\rho_n = 10^{-6}\ \Omega$ cm is assumed. This heat dissipation corresponds to about 100 cm^3 He evaporation. The measured evaporation was only slightly more, thus showing that the main contribution to the heat dissipation is given by the eddy current losses in the normal region.

These losses can be reduced by using thinner pumping bridge foils with a higher residual resistance in the normal state.

d. Pumping speed. In the application of flux pumps, the pumping speed plays a crucial role. Besides possible improvement of the pumping system, the pumping speed can also be increased by using several bridge foils in series as is drawn schematically in fig. 18. Using n foils in series, a

gain of a factor n in pumping speed is achieved, since n times the flux is brought into the circuit at every stroke. The advantage of this method of increasing the pumping speed is that no extra heat dissipation occurs in the foil. (Extra heat is dissipated if the pumping speed is increased by a larger revolution speed). This method is especially useful when a high-inductance low-current coil is connected to the pump. The important application of flux pumps, however, is to feed coils with currents in the region of several hundreds of amperes. Coils wound from Nb_3Sn wire or Nb–25% Zr cables as well as foil solenoids readily require a flux pump as a current supply.

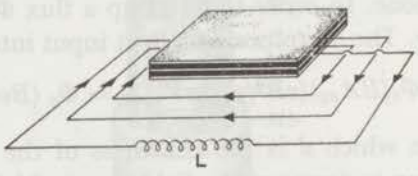

Fig. 18. Three isolated bridge foils in series connected to the coil L.

4. *Wire solenoids.* The inductance of a wire solenoid can be reduced by winding several wires in parallel. As will be shown later it is essential that all parallel circuits have equal inductances in order to get equal currents in the wires, if the coil is fed by a flux pump. This leads to the use of many-strand cables. This construction has obvious advantages such as:

a) short lengths of wire available from normal commercial production can be used;

b) lower inductive voltages at quenching of the coil, owing to a smaller total resistance. The inductive voltage occurring if the whole coil turns normal is inversely proportional to the number of strands of the cable. But if only local regions in the wires turn normal, the field energy is dissipated in these regions, which will lie in different places of the winding volume. None of our coils showed any damage after being quenched several times;

c) low-inductance coils and thus high pumping speeds;

d) a many-strand cable is, compared with a massive thick cable of the same cross-section, more easily wound and welded to the foil of the pumping bridge;

e) very little insulation material has to be used, and thus a higher filling factor can be achieved.

To stress the point made about necessary equal inductances of the parallel circuits, consider two circuits with selfinductances L_1 and L_2 respectively and with mutual inductance M_{12} (fig. 19). A flux $\Delta\Phi$ pumped into the system gives rise to a current distribution given by the equations:

$$\Delta\Phi = L_1 i_1 + M_{12} i_2$$
$$\Delta\Phi = M_{12} i_1 + L_2 i_2$$

which gives:

$$i_1 = \frac{L_2 - M_{12}}{L_1 L_2 - M_{12}^2}\,\Delta\Phi \quad \text{and} \quad i_2 = \frac{L_1 - M_{12}}{L_1 L_2 - M_{12}^2}\,\Delta\Phi.$$

Thus, if $L_1 > L_2$, then $i_1 < i_2$, which means that, when pumping is continued i_2 reaches its critical value before i_1 does. Now when circuit 2 turns normal, and thus $i_2 \to 0$, the current i_1 increases suddenly to keep the flux

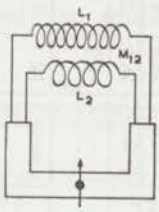

Fig. 19. Two parallel circuits with unequal selfinductances.

linked into 1 constant. Thus 1 may also go normal. It is clear that the maximum total current in a coil consisting of parallel circuits can only be achieved with equal selfinductances; thus a cable construction is obvious.

Some of our Nb–Zr wire solenoids based on these ideas are listed in table I.

For coils $W1$ and $W2$ we used a cable construction in which ten 10 mil (0.25 mm) Nb–25% Zr wires are bound together by a 4 mil stainless steel wire. With this construction the maximum current per wire of coil $W1$ for instance, corresponds to the usually achieved value of 17.5 A for this material. At the present time the fabrication of many-strand cable is followed by several industries. The pumping time of coil $W1$ and $W5$ are reduced by a factor 2 or 5 by using two or five bridge foils, respectively, in series in pump III (IV).

The selfinductances in column 11 of table I are calculated with the relation

$$L = a_1^5[A\beta(\alpha - 1)]^2\,(\alpha + 1)\left(\theta - \lambda\frac{\alpha - 1}{\beta}\right) \times 10^{-6}\ \text{(henry)}.$$

In this formula a_1 is the inner radius in cm; α and β are the ratios of outer diameter and length, respectively, to inner diameter; A is the number of turns per cm^2; and θ and λ are tabulated functions of α and β*). The average pumping speed is calculated by means of the relation $\mathrm{d}\Phi/\mathrm{d}t = Li/\tau$.

With coil $W2$ special attention was paid to the field homogeneity. A homogeneity better than 0.5% was reached for the inner 5 cm along the axis and better than 0.1% for the inner cm. This was performed by adding some extra turns of the cable near the outer ends of the coil**).

*) F. E. Terman, Radio Engineers' Handbook, Mc Graw-Hill, New York (1943), p. 60.

**) Coil $W2$ with flux pump IV has been used in our laboratory in magnetisation experiments with superconductors of the second kind.

TABLE I

Data of wire solenoids

coil No.	wire material	additional insulation	cable construction	total length of wire (m)	number of turns	length of coil (cm)	inner diameter (mm)	outer diameter (mm)	filling factor	L (mH)	number of pump	number of bridge foils	insulation between bridge foils	max field (kOe)	max current per wire (A)	pumping time τ (min)	pumping speed $d\Phi/dt$ (gauss cm²/min)
W1	[1]	[3]	[6]	10×40	10×540	4.0	6.5	39	42%	1.4	III	1	—	25.5	17.5	9	2.7×10^6
											III	2	sellotape	25.5	17.5	4.5	5.4×10^6
											III	4	none	13	8.5	saturation effect	—
											IV	1	—	25.5	17.5	3	8.0×10^6
W2	[2]	[3]	[6]	10×93	10×920	10.0	19	40	42%	4.5	IV	1	—	26.0	27	15	8.1×10^6
W3	[2]	none	2 parallel wires [7]	2×650	2×8200	15.0	14.5	35	52%		III	1	—	0[8]	0	—	
W4	[2]	[4]	single wire	1×600	8700	15.0	14.5	28	42%		III	4	none	12	17	sat. effect	
W5	[2]	[4]	2 parallel wires [7]	2×570	2×7300	15.0	14.5	37	43%	167	IV	1	—	34	28	130	7.2×10^6
												5	mylar	34	28	32	
W6	[2]	[5]	7 parallel wires [7]	7×270	7×2350	8.0	15.0	56.4	50%	47	IV	1	—	52	22	90	8.0×10^6
											IV	8	araldite				

[1] Nylon-insulated 10 mil Nb–25% Zr wire (Wah Chang).
[2] Copper-insulated 10 mil Nb–25% Zr wire (Supercon).
[3] 4 mil stainless steel wire around the cable.
[4] sellotape (60 μ thick) between the layers.
[5] Mylar (26 μ thick) between the layers.
[6] 10 wires held together by a 4 mil stainless steel wire.
[7] The indicated number of wires is wound simultaneously, the wires next to each other.
[8] An inhomogeneous field was observed with a peak value of a few hundred oersted near the ends of the coil.

The pumping speed of coil $W6$ is considerably increased by using eight 12.5 μ thick Nb bridge foils in series. The total current carried by this rather thick stack of foils however, was not nearly sufficient to reach the maximum field. The zero result on coil $W3$ shows that short-circuiting by the copper insulation can cause serious difficulties. It can be seen from the results on coils $W4$, 5 and 6 — the saturation effects with coils $W1$ and $W4$ are due to the 4 non-insulated bridge foils – that insulation only between the layers improves this already so much that these difficulties have

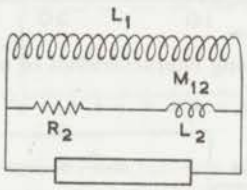

Fig. 20. A coil L_1, short-circuited by a small resistance R_2 with self inductance L_2.

disappeared. (See also the results on coil $W2$, where the stainless steel wire, with its relatively high resistance has a similar effect). These latter results can be fairly well understood. Suppose we have a coil with a selfinductance L_1 which is short-circuited by a circuit with selfinductance L_2 and resistance R_2, having a mutual inductance M_{12} with L_1 (fig. 20). If this system is fed by a current source with internal resistance $R \gg R_2$, then the current growth in the coil is determined by a time constant roughly given by L_1/R_2. If, however, the coil is fed by a flux pump without any internal resistance the time constant involved is then given by $\tau = (L_1L_2 - M_{12}^2)/L_1R_2$. In most cases, since L_2 and M_{12} are in general much smaller than L_1, τ equals L_2/R_2. Since L_2 consists mainly of the inductance from the circuit formed by the bridge and connecting leads, L_2 is of the order of 1μH. This shows that as long as the short-circuiting resistance is not much smaller than 1 $\mu\Omega$, the time constant is of the order of the pumping period and thus does not disturb seriously the pumping charateristics. This explains the negative results on coil $W3$, where the estimated short-circuiting resistance is much smaller than 1 $\mu\Omega$. With insulation between the different layers this resistance is increased by several orders of magnitude. This explains the positive results on coils $W4$, 5 and 6 (see also $W2$). Some typical pumping characteristics are given in fig. 21. Notice the change in slope corresponding to a change in selfinductance of the coil (see also section 5).

During the experiments with coils $W1$ and $W2$, we struck an interesting property which possibly shows nicely the current degradation effect. The results are shown in fig. 22 where the maximum field reached in these coils is plotted as a function of the number of wires from the outer end of the cable connected to the pumping bridge. (All wires from the inner end are connected).

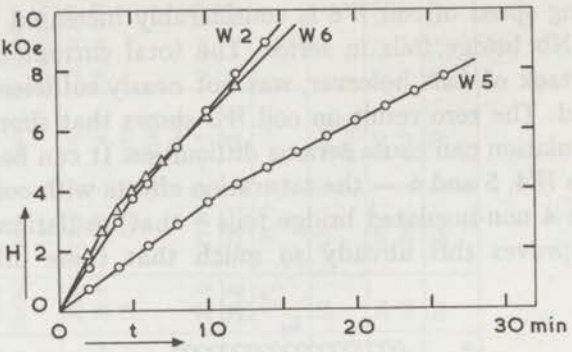

Fig. 21. Typical pumping characteristics of some wire solenoids.

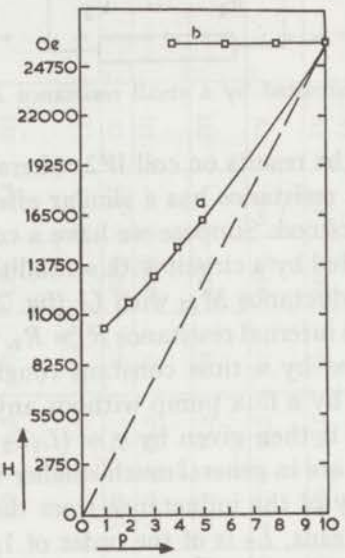

Fig. 22. Maximum fields of the coils $W1$ (*a*) and $W2$ (*b*) as functions of the number of wires p connected to the pumping bridge. We remark that in case *b*, the current can be fed into the coil by the few connected wires since their short-sample current carrying capacity is large enough to transport the total current.

Curve *a* represents the results for the nylon insulated coil $W1$, while curve *b* is the result for coil $W2$. The corresponding graph giving the current per wire as a function of the number of wires connected is shown in fig. 23 for coil $W1$. Curve *b*, fig. 22, shows that, owing to the very low contact resistance through the copper between the different members of the cable, all wires of the cable do participate in the current. For coil $W1$ the nylon insulation prevents this. For this coil the current per wire increases from the usual 17.5 A when 10 wires are connected, to the short sample value of 70 A when only one wire is connected.

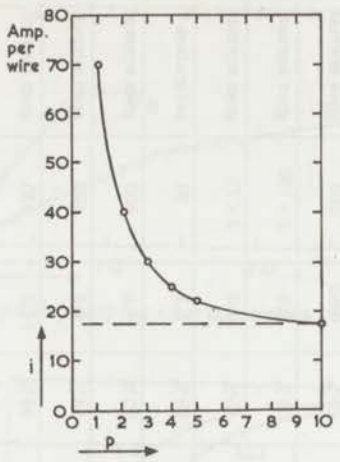

Fig. 23. The current per wire for coil $W1$ as a function of the number of wires connected to the pumping bridge.

5. *Foil solenoids.* We also tested several foil solenoids which have obvious construction advantages and a large filling factor. As material we used Pb, Pb–Hg, Pb–Bi, Nb, Nb–Zr and Nb_3Sn foil. Some of our results are listed in table II. Pumping system II was used as a current supply for all foil solenoids, the pumping times all being smaller than 20 minutes.

Coils $F1$–$F11$ were wound without any insulation between the layers. Several tests with insulated coils delivered identical results. The Nb_3Sn coils were insulated with different materials. These coils were constructed by winding a stack of foils together into a solenoid. The stack consisted of an insulating foil, a 7 μ Sn foil, a 40 μ Nb foil and another 7 μ Sn foil. This solenoid was then placed into a vacuum oven and heat treatment was given for 1 hour at 930°C. As insulating material we used either Ta foil or Nb_2O_5 foil or a ceramic material, each gave more or less identical results. In table II two arbitrary examples are given. We also constructed a coil with N.R.C. Niostan ribbon. The achieved maximum current in this coil ($F14$) in zero external field coincides with the value given by the manufacturers.

Some typical pumping characteristics are given in fig. 24. The rapid change of slopes of these characteristics can be explained by assuming that at a certain critical field B^* a gradual change in selfinductance of the coil sets in. This is due to the fact that the field starts to penetrate step by step into the bulk of the successive windings, Assuming a constant input per time unit $d\Phi/dt$, the slope is no longer determined by the relation $d\Phi/dt = L\, di/dt$ but by $d\Phi/dt = L\, di/dt + i\, dL/dt = (L + i(dL/di))\, di/dt$. Thus a sudden change in the slope of the pumping characteristics occurs. The results of a numerical calculation of the selfinductance L as a function of the reduced field B/B^* and of the pumping characteristics respectively are

TABLE II

coil No.	foil material	thickness foil (μ)	contact to pumping bridge	type of bridge	length coil (cm)	inner diameter (mm)	outer diameter (mm)	number of turns	filling factor	max field (kOe)	max current (A)	behaviour at maximum level
*F*1	Pb	600	Woods metal	Pb	2.0	17	34	12	88%	0.34	75	saturation
*F*2	Pb–Bi (eut.)	1000	Woods metal	Pb	2.0	17	32	7	94%	0.30	105	saturation
*F*3	Pb–15% Hg	600	Woods metal	Pb Pb–Hg	2.0	17	32	10	80%	0.36	90	saturation
*F*4 [1]	Pb–15% Hg	600	Woods metal	none	2.0	15	15.6	1	—	0.12	360	saturation
*F*5	Nb [3]	50	Seam-less	Nb (50μ)	2.5	30	31	7.5	75%	0.60	250	goes normal
*F*6	Nb [3]	50	Seam-less	Nb (50μ)	2×1.0	19	25	35	58%	2.8	2×100	goes normal
*F*7	Nb [3]	50	Seam-less	Nb (50μ)	2×1.0	10	18	52	65%	4.0	2×75	goes normal
*F*8	Nb [3]	50	spot welding	Nb (50μ)	2.0	10	24.5	127	88%	5.2	90	saturation
*F*9	Nb–25% Zr [4]	110	spot welding	Nb (200μ)	3.8	11.6	21.6	41	90%	9.6	800	goes normal
*F*10	Nb–25% Zr [4]	110	spot welding	Nb (200μ)	3.8	7.0	19.0	51	94%	9.8	620	goes normal
*F*11	Nb–25% Zr [4]	140	spot welding	Nb (200μ)	5.0	14.0	45	104	94%	14.0	620	goes normal
*F*12	Nb_3Sn		spot welding [2]	Nb (200μ)	1.0	10.0	12	11		5.5	540	goes normal
*F*13	Nb_3Sn		spot welding [2]	Nb (200μ)	1.0	10.0	15.0	37		10.0	270	goes normal
*F*14	Nb_3Sn [5] (Niostan)	60	spot welding [2]	Nb	1.3	10	14.0	31	93%	7.5	300	goes normal

[1]) This coil is a single cylinder as in fig. 14.

[2]) The connection to the Nb pumping bridge was formed by 10 Nb–Zr wires, spot welded outside the field to the coil and to the bridge.

[3]) Niobium foil of Kawecki-Billiton, thickness 50μ.

[4]) Niobium–25% zirconium foil of Kawecki, thickness 110μ(*F*9, *F*10) and 140μ (*F*11).

[5]) Niostan, N.R.C. (The National Research Corporation prepares Nb_3Sn ribbon by first coating Nb foil with molten Sn and then reacting them at elevated temperature to form a few-tenths-of-a-mil-thick Nb_3Sn layer on the surface. The ribbons can be wound into solenoids without further heat treatment).

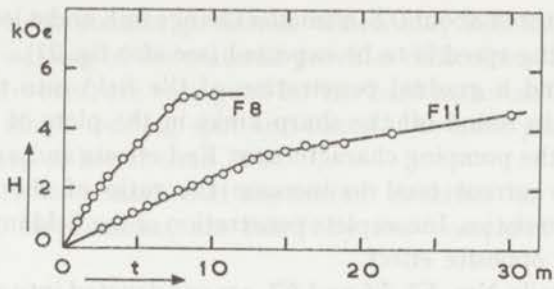

Fig. 24. Typical pumping characteristics of foil solenoids.

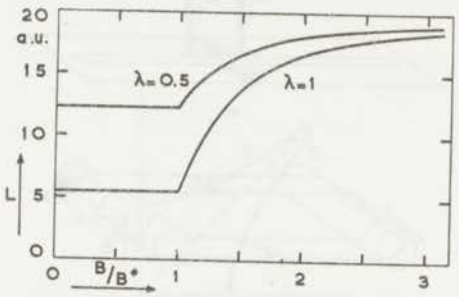

Fig. 25. Calculated selfinductance L as a function of the reduced field B/B^* for a coil of the same dimensions as $F11$, for a space factor $\lambda = 0.5$ and $\lambda = 1$.

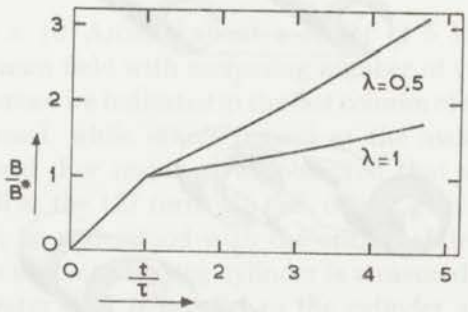

Fig. 26. Calculated pumping characteristic for a coil of the same dimensions as $F11$ for $\lambda = 0.5$ and $\lambda = 1$.

plotted in figs. 25 and 26. These results are for coil $F11$, which has a relatively large ratio of outer to inner diameter. End effects are neglected, and it is assumed that complete penetration of the field into the bulk of a winding takes place instantaneously when the field inside this winding reaches the value B^*. B^* was taken independent of the current. The actual coil $F11$ has a filling factor λ of nearly 1. The effect of λ is shown by also plotting in figs. 25 and 26 the results for a coil of the same dimensions, but now with a filling factor $\lambda = 0.5$. This shows that for wire solenoids, which usually

have a filling factor of about 0.5, a smaller change in L and a less pronounced change in pumping speed is to be expected (see also fig. 21).

End effects and a gradual penetration of the field into the volume of a winding tend to round off the sharp kinks in the plots of both the self-inductance and the pumping characteristic. End effects and a decrease of B^* with increasing current tend to increase the ratio of the slopes of the pumping characteristics. Incomplete penetration of the field into the winding volume has the opposite effect.

The seamless coils, Nos. $F5$, $F6$ and $F7$, are constructed into a closed circuit from one piece of foil as is sketched in figs. 27*a*, *b*, *c*, *d* and *e*. This type of

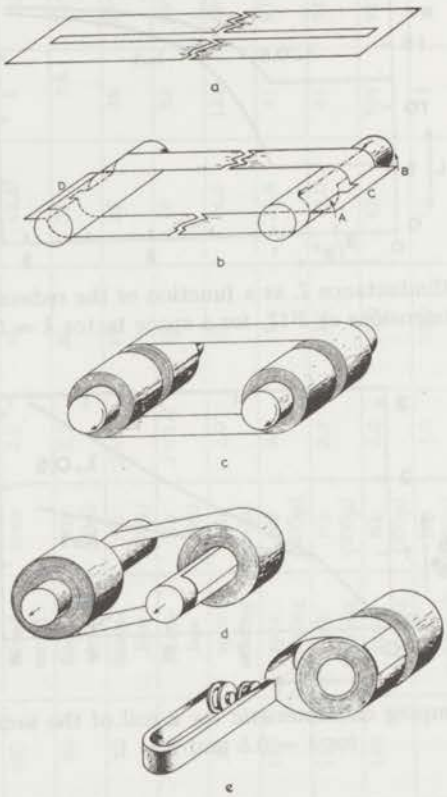

Fig. 27. The procedure of the construction of a seamless foil solenoïd.

a. A strip of foil is lengthwise cut in two halves of equal width without cutting the ends.

b. Two cylinders A and B are inserted between the two halves, and the ends of the foil are folded against these cylinders.

c. As the cylinders are turned, the foils are twisted in opposite directions. This gives 4 coils.

d. By turning the cylinders in the same direction 2 coils are obtained.

e. The cylinders are removed, and the coils are put together.

construction avoids contact problems, which may become of importance in cases where welding of the material provides difficulties. The results with spot welding, however, are very good for the hard materials Nb and Nb–Zr. We tested one single welding spot and found it to have persistent current carrying capacity of better than 70 A.

From table II we remark that the current densities for the Nb–Zr foils ($\approx 10^4$ A/cm^2), for instance, are relatively low compared with those of

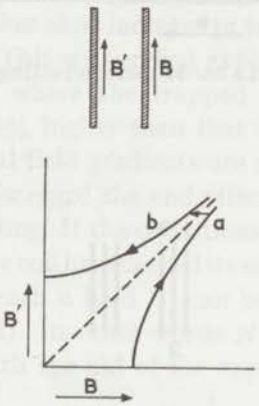

Fig. 28. The critical state curves for a superconducting cylinder in an applied field B.

Nb–Zr wires ($\approx 5 \times 10^4$ A/cm^2), about a factor of 5 lower. Also the increase of the maximum field with increasing number of turns is disappointingly slow. Furthermore we indicated in the last column of the table that some of our coils go normal, while others remain at the maximum level when pumping is continued. For instance, we observed that all our Pb–Bi and Pb–Hg coils, as well as the 127 turns Nb coil, do not go normal.

These effects can be understood with the critical-state theory [32]). When the field B' inside a superconducting cylinder is measured as a function of a slowly increasing outer field B parallel to the cylinder axis, one measures curve a of fig. 28. On decreasing the outer field B, B' follows the upper curve b. The relation between B and B' can be described by the empirical expression, $I_c(B + B_0) = \alpha_c$, where I_c is the critical current density in a field B and α_c and B_0 are constants of the material. This expression leads to the two experimentally verified hyperbolae a and b which are given by $(B' + B_0)^2 - (B + B_0)^2 = \pm 2\alpha_c kw$. In this relation, w is the wall thickness of the cylinder and k is a constant with a value depending on the units used. The quantity k equals $4\pi \times 10^{-4}$ kOe cm (A)$^{-1}$ if B and B_0 are expressed in kOe, w in cm and α_c in A kOe/cm^2. When hard materials are used flux jumps distort this picture considerably for lower fields so that one gets a behaviour as is sketched in fig. 29. Jumps occur between the critical state

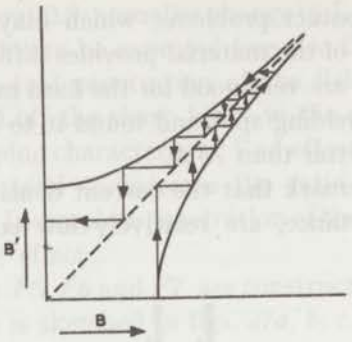

Fig. 29. Flux jumps occurring in a hard superconducting cylinder in an applied field B.

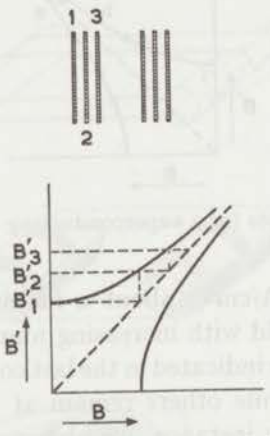

Fig. 30. The behaviour of 3 identical cylinders, placed inside each other, in an applied field B.

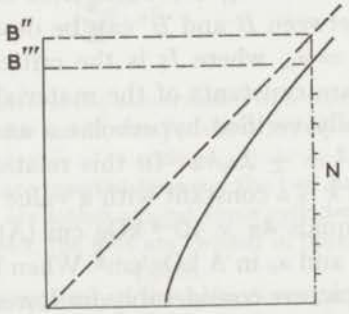

Fig. 31. The number of windings of a foil solenoïd necessary to reach a field B''.

curves and the complete field penetration curve (45°-line) at lower fields. In the higher field region, the region of the so-called flux creep, the critical state curves are followed. In this picture the behaviour of 3 identical cylinders placed inside each other will be, if we disregard end effects and flux jumps, as sketched in fig. 30. Here it is supposed that we have cooled these cylinders down under their critical temperature in the presence of a large magnetic field and then slowly have decreased the field to zero. The outer cylinder will trap a field B_1'. The second cylinder thus sees an external field B_1' and thus can trap a field B_2'. The inner cylinder traps in the same way a field B_3'. From fig. 30 we see the rather slow increase in trapped field with increasing number of cylinders used. This we verified experimentally with two nearly identical Nb_3Sn cylinders where the trapped field of the two cylinders together was only about 25% higher than that of the cylinders separately.

For a coil, however, equal field gradients are necessary over the different windings when we again disregard the end effects. This is due to the equal currents through each winding. If the conditions for the inner winding have reached the critical state, the coil has reached its maximum value. The number of windings necessary to reach a field B'' can be read from the plot of the critical state curves (fig. 31). In other words $N = B''/(B'' - B''')$, and this can easily be calculated with the aid of the expression for the hyperbolae.

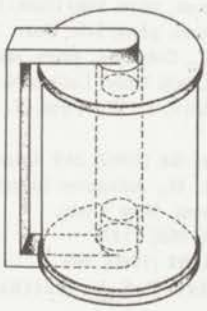

Fig. 32. Coil $F11$ with a soft iron yoke.

If B''' lies in the region of flux jumps, the lower field region, the coil can go normal. But if B''' lies in the region of flux creep, the field remains nearly constant and the coil does not go normal when flux pumping is continued. These considerations explain nicely the disappointingly low increase of maximum field with number of turns as well as the behaviour at the maximum level. But they also deliver the low value of α_c of 2×10^5 kOe A/cm^2 for the Nb–Zr foils; this compares rather poorly with the measured values of 10^6 to 5×10^6 for Nb–Zr wires.

That end effects also play an important role is demonstrated with coil No. $F11$, in which a soft iron yoke is placed in the way sketched in fig. 32.

A gain of 30% in maximum field value was achieved in this way bringing the maximum field to 18 kOe. The distance between the poles of the yoke was about 4 cm, large enough not to give an increase of field of that order of magnitude. The function of the yoke is merely to concentrate the field lines, thus changing the end conditions.

The extent to which end effects are responsible for the low value of α_c and how far these values of α_c can be improved (by heat treatment or copper plating of the Nb–Zr foils for example) are still under investigation.

To conclude this chapter we remark that there is already a great assortment of flux pumps and current generators to choose from as current supplies for superconducting magnets. If we accept that the main merits of a flux pump are given by its pumping speed, current carrying capacity, heat dissipation and simplicity, this article shows that there are already several applicable pumps of comparable performance. A definite choice cannot be made. However, in our opinion flux pumps could play an important role in the future of superconductivity.

REFERENCES

1) Kamerlingh Onnes, H., Commun. phys. lab. Univ. Leiden No. 122*b* (1911).
2) Kamerlingh Onnes, H., Commun. phys. lab. Univ. Leiden No. 133*d* (1913).
3) De Haas, W. J. and Voogd, J., Commun. phys. lab. Univ. Leiden No. 214*b* (1931).
4) Keesom, W. H., Commun. phys. lab. Univ. Leiden No. 234*f* (1935).
5) Rjabinin, J. N. and Schubnikov, L. W., Phys. Z. Sowjet **7** (1935) 122; Nature (London) **135** (1935) 581.
6) Autler, S. H., Rev. sci. Instrum. **31** (1960) 369. Comment by S. H. Autler on the paper of Arp, V. D. and Kropschot, R. H., Advances in cryogenic Engineering **6** (1961) 888, Ed. K. D. Timmerhaus (Plenum Press, New York).
7) Yntema, G. B., Phys. Rev. **98** (1955) 1197.
8) Autler, S. H., Rev. sci. Instrum. **31** (1960) 369.
9) Kunzler, J. E., Buehler, E., Hsu, F. S. L., Matthias, B. T. and Wahl, C., J. appl. Phys. **32** (1961) 325.
10) Matthias, B. T., Phys. Rev. **92** (1953) 874.
11) Matthias, B. T., Geballe, T. H., Geller, S. and Corenwitz, E., Phys. Rev. **95** (1954) 1435.
12) Berlincourt, T. G., Hake, R. R. and Leslie, B. H., Phys. Rev. Letters **6** (1961) 671.
Aron, P. R. and Hitchcock, H. C., J. appl. Phys. **33** (1962) 2242.
13) Kunzler, J. E., Buehler, E., Hsu, F. S. L. and Wernick, J. H., Phys. Rev. Letters **6** (1961) 89.
14) Riemersma, H., Hulm, J. K., Venturino, A. J. and Chandrasekhar, B. S., J. appl. Phys. **33** (1962) 3499.
15) Martin, D. L., Benz, M. G., Bruch, C. A. and Rosner, C. H., Cryogenics **3** (1963) 114.
16) Westinghouse HI-120 wire.
17) Schrader, E. R., Freedman, N. S. and Fakan, J. C., Appl. Phys. Letters **4** (1964) 105.
Recently 107 kOe is reached.
18) Mendelssohn, K., Nature (London) **132** (1933) 602.
19) Olsen, J. L., Rev. sci. Instrum **29** (1958) 537
Buchhold, T., Cryogenics **4** (1964) 212.

20) Swartz, P. S. and Rosner, C. H., J. appl. Phys. **33** (1962) 2292.
Hildebrandt, A. F., Elleman, D. D., Whitmore, F. C. and Simpkins, R., J. appl. Phys. **33** (1962) 2375.
Elleman, D. D. and Hildebrandt, A. F., Proc. 8th Int. conf. on low temperature physics (Butterworth, London, 1963) p. 332.
21) Laquer, H. L., Cryogenics **3** (1963) 27.
22) Marchand, J. F. and Volger, J., Phys. Letters **2** (1962) 118.
23) Volger, J. and Admiraal, P. S., Phys. Letters **2** (1962) 257; Phil. techn. Tijdschrift **25** (1963) 16.
24) Vollgraff, J. A., Electromagnetische draaiingen en unipolaire inductie. (Thesis Leiden(1903) in Dutch).
25) A description of this flux pump was sent on 14 February 1963 as a preprint to the XIth International congress on refrigeration, Munich (1963).
26) Van Beelen, H., Arnold, Miss A. J. P. T., De Bruyn Ouboter, R., Beenakker, J. J. M. and Taconis, K. W., Phys. Letters **4** (1963) 310.
27) Van Beelen, H., Arnold, Miss A. J. P. T., Sypkens, H. A., Van Braam Houckgeest, J. P., Beenakker, J. J. M., De Bruyn Ouboter, R. and Taconis, K. W., Proc. of the Conf. on the phys. of type II superconductivity (Cleveland, Ohio, U.S.A., 1964) Vol. 2, p. IV–53.
28) See for boundary conditions in a moving system: Landau, L. D. and Lifshitz, E. M., Electrodynamics of continuous media (Pergamon press, London, 1962) p. 177 and 178.
29) Wipf, S. L., Advances in cryogenic Engineering **9** (1964) 342, Ed. K. D. Timmerhaus (Plenum Press, New York).
30) Van Houwelingen, D., Admiraal, P. S. and Van Suchtelen, J., Phys. Letters **8** (1964) 310.
31) Van Beelen, H., Arnold, Miss A. J. P. T., Sypkens, H. A., De Bruyn Ouboter, R., Beenakker, J. J. M. and Taconis, K. W., Phys. Letters **7** (1963) 175.
32) Bean, C. P., Phys. Rev. Letters **8** (1962) 250. Anderson, P. W., Phys. Rev. Letters **9** (1962) 309. Kim, Y. B., Hempstead, C. F. and Strnad, A. R., Phys. Rev. **129** (1963) 528.
33) Voigt, H., Z. Naturforsch. **21a** (1966) 510.
34) Weber, R., Z. angew. Phys. **22** (1967) 449.

REMARKS ON A MOVING-FLUX EXPERIMENT IN SUPERCONDUCTING SHEETS

Synopsis

In order to study the voltages, associated with flux motion in a superconductor, a rotating magnet experiment is described. It is shown that the results obtained with a type-II superconductor can be explained by its resistive behaviour in the mixed state, as measured by means of a transport current. It is argued that the interaction between a moving applied field and the circulation currents of the vortices only takes place through the induced eddy currents in the sample. A discussion of the observed voltages due to flux motion leads to the conclusion that independent of the equation of motion of the flux tubes, the measured electric field strength $\boldsymbol{E} = -\boldsymbol{v}_\Phi \times \boldsymbol{B}$, where $\boldsymbol{v}_\Phi$ is the velocity of the flux tubes and $\boldsymbol{B}$ the average magnetic induction in the sample. Flux pinning influences strongly the results obtained in the niobium specimens. The conclusions drawn for the eddy currents, generated in the sample, are tested with an experiment in which the forces, excerted on a niobium cylinder rotating in an inhomogeneous magnetic field, are measured.

1. *Introduction.* In the last few years much attention has been paid to the problem of moving flux patterns in superconductors[1–13]), both of type I and of type II. The problem can be summarised in two main questions:

1) What is the equation of motion for the flux pattern? What is the balance of forces, working on a stationary moving flux tube[1–7]) in a pinning free sample?
2) If the velocity of motion is known, what are the observed voltages?[1–13])*)

In this chapter we will comment only on the second question.

The voltages, arising in the presence of a transport current and a perpendicularly applied magnetic field[14]) both transverse and longitudinal to the current, do not give an answer to these questions separately. If, however, the answer to one of the questions were known, experiment could decide

*) One could even wonder whether the second question has a unique answer. A certain flux motion can be induced by different causes, for instance by a transport current or by a moving magnetic field. Are the measured voltages the same in both cases? We will show that such an ambiguity does not exist.

upon the other, at least in principle. Flux pinning, however, will confuse the answer.

It seemed therefore useful to design an experiment in which a well-known velocity is imposed on the flux pattern and the generated voltage is measured. As this goal cannot be achieved with a resistance or Hall experiment, that means by driving a current through the sample, one can try to reach it by a moving magnetic field method, in which the flux pattern is dragged along at the speed of the moving magnet. The ideal experiment would be to have a homogeneous flux pattern, moving at a known velocity. It is clear, however, from a simple argument, that the motion of a homogeneous magnetic field cannot realise such a situation. The external conditions, which determine the flux distribution in equilibrium, do not change anywhere in the sample by such a displacement. A picture in which the vortices in a type-II superconductor are rigidly connected to the pole pieces of the magnet by the magnetic lines of force, is misleading (fig. 1*a*). Actually, the total field pattern can be considered as the sum of the applied field, corrected for the field associated with the Meissner current along the edge of the sample, and

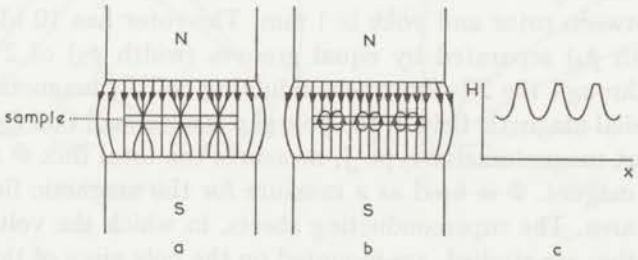

Fig. 1. Sketch of the field configuration for a specimen in the mixed state.
a) the total field.
b) the two components, the applied field (Meissner field being neglected) and the field belonging to the circulation current of the vortex.
c) the total field in the specimen in a plane through the centres of the vortices.

the closed field pattern belonging to the circulation currents around the vortex cores (fig. 1*b*). There are no interacting forces between the vortices and the moving homogeneous applied field. Besides, it should be remarked, that if a vortex moves in a thin sheet (*e.g.* as a consequence of a transport current), there is no net flux transport connected with this motion as its closed field pattern carries no net flux on a scale of the order of the thickness of the sheet. In order to obtain a moving flux pattern by moving an externally applied magnetic field, it is thus necessary to use an inhomogeneous external field. In section 2 we will describe such an experiment. Section 3 gives the results obtained. A general discussion of measured voltages due to flux motion will be given in section 4. Section 5 will give a discussion of the experimental results.

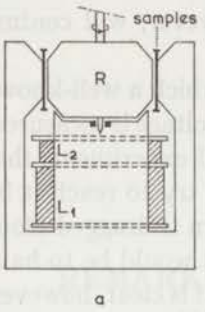

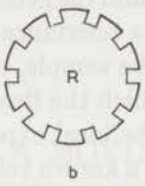

Fig. 2

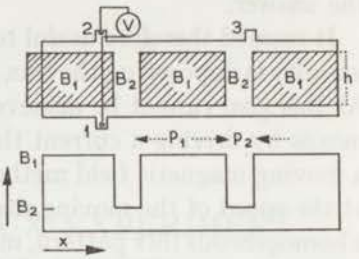

Fig. 3

Fig. 2. The apparatus.

Fig. 3. *a*) Unfolded view of the superconducting foil in the magnetic field. The voltmeter connections are shown.
b) The idealised rectangular field pattern.

2). *The experiment.* The moving magnetic field is obtained with the apparatus sketched in figure 2. The magnet consists of a soft-iron yoke of circular symmetry and a soft-iron rotor R, mounted as indicated. The pole gap between rotor and yoke is 1 mm. The rotor has 10 identical pole pieces (width p_1) separated by equal grooves (width p_2) of 2 mm depth. A current through the Nb–Zr superconducting coil L_1 magnetises the iron so that a radial magnetic field in the pole gap is obtained. Coil L_2, connected to a Newport magnetometer type J, measures the total flux Φ through the core of the magnet. Φ is used as a measure for the magnetic field strength in the pole area. The superconducting sheets, in which the voltages due to the flux motion are studied, are mounted on the pole piece of the yoke. The applied magnetic field pattern obtained in this way is shown schematically in fig. 3. The voltmeter V is connected in such a way that no induction voltages occur due to flux changes in the voltmeter circuit (see fig. 3*a*). The voltages, measured as a function of Φ for different speeds of rotation, are amplified by a Hewlett-Packard null voltmeter, type 419 DC, from which the output is recorded as a function of Φ on a Moseley x–y recorder, type 135 AM.

We used three different rotors, with different pole piece to groove ratio's, as given in table I. The ratios of the fields opposite pole piece and groove

TABLE I

Rotor	Pole p_1 (mm)	Groove p_2 (mm)	B_1/B_2
I	3.3	6	3.0
II	5.3	4	2.0
III	7.3	2	2.0

are also given in this table. (We will use the index 1 for all quantities related to the high-field area in the pole gap, the index 2 in connection with the groove).

The results obtained on specimens with a height (14 mm) larger than the height of the pole gap h (9 mm) will be discussed. As samples we used a 100 μ-thick niobium foil ($\rho_{300}/\rho_{20} \approx 26$) and a 25 μ-thick tantalum foil ($\rho_{300}/\rho_{20} \approx$ ≈ 17).

3. *Experimental results.* The measured direct voltage $\overline{V}$ in our Nb-foil is shown, as a function of Φ, in fig. 4. The linear velocity is 0.70 m/s and $T = 4.2°K$. The curve for the three different rotors is given. Upon reducing the speed of rotation, the voltages decrease but the essential features of

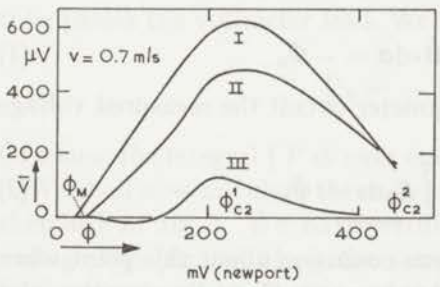

Fig. 4

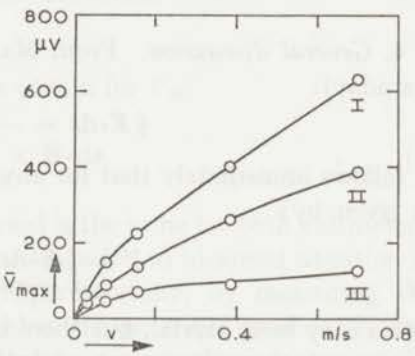

Fig. 5

Fig. 4. The measured direct voltage across a 100 μ-thick Nb-foil for three different rotors ($v = 0.7$ m/s).

Fig. 5. The peak height $\overline{V}_{max}$ as a function of the velocity, given for three different rotors.

fig. 4 remain the same. In fig. 5 the peak height $\overline{V}_{max}$ is plotted against v for the different rotors. The direct voltages are in reality the averaged values of periodically varying voltages. At high speeds ($v = 0.05 - 0.70$ m/s) the periodic voltages can be displayed on an oscilloscope, at lower speeds with the recorder. An example of the latter is given in fig. 6, where the voltages are shown, obtained with rotor III, for two different field values, one between Φ_M and Φ^1_{c2}, where $\overline{V}$ is negative (see fig. 4), and one between Φ^1_{c2} and Φ^2_{c2}. At low speeds the direct voltage can be obtained by integration of the recorded $V - t$ curves. Qualitatively similar results are obtained in the tantalum specimen (fig. 7), only no change of sign occurs in $\overline{V}$ for any of the rotors. The peak height $\overline{V}_{max}$ is in these samples very nearly proportional to the speed of rotation. The obtained $\overline{V} - \Phi$ characteristics at different temperatures are almost conform with respect to the origin.

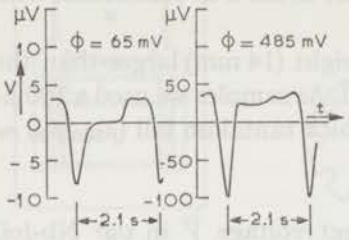

Fig. 6

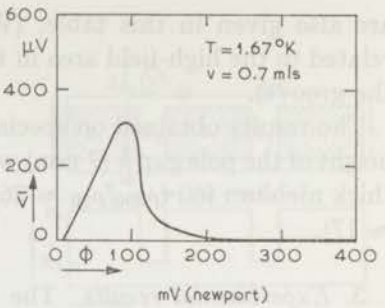

Fig. 7

Fig. 6. The alternating voltage as a function of time recorded for rotor III.
a) $\Phi_M < \Phi < \Phi_{c2}^1$ *b)* $\Phi_{c2}^1 < \Phi < \Phi_{c2}^2$. $(v = 4.5 \times 10^{-3}$ m/s).
Fig. 7. The direct voltage for rotor I in a 25 μ-thick Ta-foil. ($v = 0.7$ m/s, $T = 1.67$°K).

4. *General discussion.* From Maxwell's equation (the induction law of Faraday):

$$\oint \boldsymbol{E} \cdot \mathrm{d}\boldsymbol{s} = -\iint \dot{\boldsymbol{B}} \cdot \mathrm{d}\boldsymbol{a} = -\dot{\Phi}_a \tag{1}$$

it follows immediately that for any voltmeter circuit the measured voltage is given by:

$$V = \int_1^2 \boldsymbol{E} \cdot \mathrm{d}\boldsymbol{s} = \int_{1\ \text{voltmeter}}^{2} \boldsymbol{E} \cdot \mathrm{d}\boldsymbol{s} + \dot{\Phi}_a. \tag{2}$$

(This may seem trivial, but there is some confusion about this point when superconductors are concerned [1–13]). Applying eq. (2) to the situation of a large moving flux tube (fig. 8*a*) surrounded by completely superconducting material, as is encountered in the Leiden flux pump[15]) for instance, leads to a voltage measured by V_a:

$$V_a = \int_1^2 \boldsymbol{E} \cdot \mathrm{d}\boldsymbol{s} + \dot{\Phi}_a = 0, \tag{3}$$

since no flux enters the circuit ($\dot{\Phi}_a = 0$) and along path I through the superconducting material the electric field strength $\boldsymbol{E} = 0$. (It is evident that for a different path through the foil the same result, $V_a = 0$, is obtained). That this is what actually happens is clearly demonstrated in fig. 9. In this figure the field inside a low-inductance superconducting coil is plotted against time during the flux-pumping process. (The superconducting coil has replaced voltmeter V_a of fig. 8*a*). It is clear from this diagram that *there is no net increase of flux* (*no direct voltage*) *during the motion of the flux tube through the foil.* Only when the pumping field is reversed inside the circuit the coil field increases. We remark that voltmeter V_b (fig. 8*b*) *does* measure a voltage during the motion of the flux tube. Again $\boldsymbol{E} = 0$ along path I, but $\dot{\Phi}_a = -\int_{1\ \text{lead}}^{2} \boldsymbol{v}_\Phi \times \boldsymbol{B} \cdot \mathrm{d}\boldsymbol{s}$ which is unequal to zero when the flux

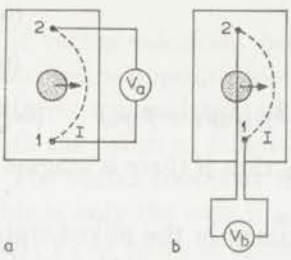

Fig. 8

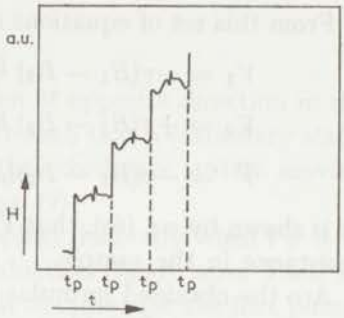

Fig. 9

Fig. 8. Two different voltmeter connections for measuring the voltage across a foil in which a large flux tube is moving (flux pump).

Fig. 9. The field in a superconducting coil during a pumping cyclus. At t_p the pumping field is reversed inside the circuit.

tube passes the voltmeter lead. We thus obtain for V_b:

$$V_b = -\int_{1\ \text{lead}}^{2} \boldsymbol{v}_\phi \times \boldsymbol{B} \cdot \mathrm{d}\boldsymbol{s}. \tag{4}$$

Of course the integral $\int V\,\mathrm{d}t$ over one period is the same for both voltmeters.

We shall now calculate the measured voltage for an idealised situation as sketched in fig. 3. We have verified experimentally, by measuring the voltage V_{23} (fig. 3*a*) along the sample, that the potential gradient is zero in the upper and lower strips of the specimen, outside the pole area of the magnet. These strips thus provide for a uniform potential difference $\Delta\varphi$ across the sample. We assume for simplicity that the field pattern, moving at the speed v of the rotor, is rectangular, as sketched in fig. 3*b*. If the ratios of electric field and current density opposite pole piece and groove are ρ_1 and ρ_2 respectively, we can derive the measured voltages V_1, V_2 and $\overline{V}$ from the complete set of equations:

$$V_1 = \int_1^2 \boldsymbol{E}_1 \cdot \mathrm{d}\boldsymbol{s} + \dot{\Phi}_a = (-\boldsymbol{v} \times \boldsymbol{B}_1 - \boldsymbol{V}\varphi) \cdot \boldsymbol{h} \tag{5a}$$

$$V_2 = \int_1^2 \boldsymbol{E}_2 \cdot \mathrm{d}\boldsymbol{s} + \dot{\Phi}_a = (-\boldsymbol{v} \times \boldsymbol{B}_2 - \boldsymbol{V}\varphi) \cdot \boldsymbol{h} \tag{5b}$$

$$\boldsymbol{E}_1 = \rho_1 \boldsymbol{I}_1 \tag{5c}$$

$$\boldsymbol{E}_2 = \rho_2 \boldsymbol{I}_2 \tag{5d}$$

$$p_1 \boldsymbol{I}_1 + p_2 \boldsymbol{I}_2 = 0 \tag{5e}$$

$$(p_1 V_1 + p_2 V_2)/(p_1 + p_2) = \overline{V}. \tag{5f}$$

(The influence of a possible Hall effect has been neglected).

From this set of equations one obtains by simple algebra:

$$V_1 = -v(B_1 - B_2)\, hp_2\rho_1/(p_2\rho_1 + p_1\rho_2) \tag{6a}$$

$$V_2 = +v(B_1 - B_2)\, hp_1\rho_2/(p_2\rho_1 + p_1\rho_2) \tag{6b}$$

$$\overline{V} = -v(B_1 - B_2)(\rho_1 - \rho_2)\, hp_1p_2/(p_1 + p_2)(p_2\rho_1 + p_1\rho_2) \tag{6c}*)$$

It is shown by eq. (6c), that $\overline{V} \neq 0$ only if $\rho_1 \neq \rho_2$, thus if there is magnetoresistance in the sample.

Are the obtained formulae applicable to a specimen in the mixed state? Does the magnetic field move at the speed of the rotor even if the vortices do not move at this speed? As has been pointed out in section 1, one can consider the total field as the superposition of the applied field and the field of the vortices. The applied field moves over the sample as in fig. 3*b*. The electric field, induced by this motion, builds up a potential difference over the foil and, secondly, as the applied field is not homogeneous, it generates eddy currents, which alter slightly the moving induction pattern (see fig. 6). Since the applied field can exert no resulting force on the vortices, it must be the eddy currents which drag the vortices along with the applied field, at speeds determined through the equation of motion by the local current densities. The advantage of this type of experiment over a resistance measurement has thus vanished as the motion of the vortex pattern is not known and an answer to question 2 of section 1 cannot be obtained. One can even wonder whether the two questions can be separated at all, since we have just argued that *only a current can exert a driving force on a vortex.* (Changing an equilibrium vortex distribution is always accompanied by a current). What do we find for the vortex velocity if we apply the commonly used expression for vortex motion in a pinning free sample[1–14]):

$$\boldsymbol{I} \times \boldsymbol{\Phi}_0 = \eta \boldsymbol{v}_\Phi \tag{7}$$

for the component of motion perpendicular to the current? In this formula $\boldsymbol{I}$ is the applied current density, η is a friction coefficient, $\boldsymbol{\Phi}_0$ the unit of flux and $\boldsymbol{v}_\Phi$ the vortex velocity. Eq. (7), together with the dissipation relation:

$$I^2\rho = n\eta v_\Phi^2 = \frac{B}{\Phi_0}\eta v_\Phi^2,$$

leads to a specific resistance:

$$\rho = B\Phi_0/\eta \tag{8}$$

so that we obtain for the local vortex velocity $v_{\Phi i}$ ($i = 1$ or 2):

$$v_{\Phi i}B_i = I_i\Phi_0B_i/\eta_i = \Phi_0B_iE_i/\eta_i\rho_i = (vB_i + \nabla\varphi)\, B_i\Phi_0/\rho_i\eta_i = vB_i + \nabla\varphi$$

*) One could ask whether the total induction is moving or just the nonuniform part of the field, B_1–B_2. This question is not relevant as far as the measured voltages are concerned.

and thus

$$v_{\Phi i} = v + V\varphi/B_i. \tag{9}$$

The vortex velocities, being different and even of opposite direction in the two regions opposite pole piece and groove, are such that a stationary state, with no accumulation of vortices, results in the coordinate system moving with the rotor, as follows immediately from eq. (9).

The vortex moves at the velocity of the applied field only when $V\varphi = 0$. This is only the case if ρ_2 and the moving induction B_2 are zero. Then we find: $V_1 = vB_1h$, in accordance with the result obtained for the flux pump, eq. (4), while we know $v_{\Phi 1} = v$. This result, obtained using eq. (7) is of course independent of the equation of motion! The vortex pattern moves with the magnetic induction in this case ($B = n\Phi_0$) and the measured voltage is merely determined by the total flux transport, to which the vortices as such do not contribute. For this special case ($B_2 = 0$, $\rho_2 = 0$) we now have obtained the answer to question 2, since we know the vortex motion in this thought-experiment, and we know the measured voltage. However, does this answer apply to all situations? There may be some doubt, since, in this experiment, the motion of the magnetic induction in the sample is responsible for the measured voltages, rather than the vortex motion. The resistance mechanism, which accompanies the vortex motion, merely permits the induction to move. In a perfect conductor the eddy currents, induced by a moving applied field, do not dissipate heat and the induction in the specimen is not able to move. In the case of the moving vortices, however, there is dissipation and the induced eddy currents stabilise on such a value that:

$$-\dot{\Phi}_a = \oint \boldsymbol{I}\rho \,.\, \mathrm{d}\boldsymbol{s} = -\oint (\boldsymbol{v}_\Phi \times \boldsymbol{B}_1) \cdot \mathrm{d}\boldsymbol{s} \tag{10}$$

for any path through the mixed-state area, which closes through the exterior superconducting region. As only this current is responsible for the vortex motion (see before) with velocity $\boldsymbol{v}_\Phi = \boldsymbol{v}$, we conclude that the measured voltage only depends on the density of the current, and is unaffected by the question whether this current is generated by an external battery or by a moving applied field. The unambiguous answer to question 2 is thus:

$$V_m = -\int_a (\boldsymbol{v}_\Phi \times \boldsymbol{B}) \cdot \mathrm{d}\boldsymbol{s} \tag{11}$$

where $\boldsymbol{v}_\Phi$ is the velocity of the vortex pattern and $\boldsymbol{B}$ the average magnetic induction in the sample *).

5. *Discussion of the experimental results.* We have shown that, in order to interpret our experimental results, we can use the derived formulae (6*a*),

*) That this result can also be obtained from the equation of motion of the superfluid will be shown in chapter III.

(6*b*) and (6*c*) for V_1, V_2 and $\overline{V}$, in which the ρ's are now the usual mixed state specific resistances. From eq. (6*c*) follows that the nonlinear behaviour of $\overline{V}$ as a function of the applied field, is determined by the factor $(\rho_1 - \rho_2)/(\rho_1 + \rho_1\rho_2/\rho_2)$. For instance, the change of sign in $\overline{V}$ for rotor III simply means that $\rho_1 - \rho_2$ changes sign in this region. From eq. (6*a*) and (6*b*) follows that:

$$V_1 - V_2 = v(B_1 - B_2)\, h \tag{12}$$

which is independent of the ρ's. This quantity, divided by vh, is plotted in fig. 10 for rotor III. From this figure we notice, that up to a rather large value Φ_M, of the flux through the core of the magnet, $V_1 - V_2$ remains zero and thus $B_1 - B_2 = 0$. This value of Φ_M would correspond to an applied field of roughly 600 gauss if no superconducting foil was in-

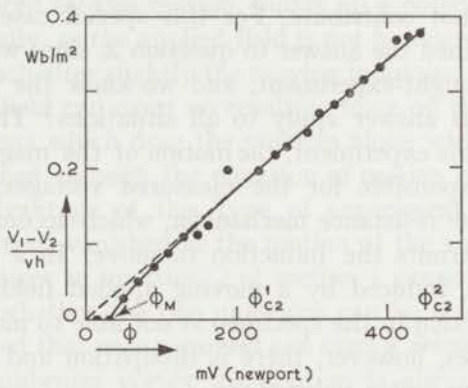

Fig. 10. The quantity $(V_1 - V_2)/vh = B_1 - B_2$ as a function of Φ for rotor III and a 100 μ-thick Nb-foil ($v = 3.6 \times 10^{-3}$ m/s).

serted in the narrow pole gap. If indeed the applied field would be 600 gauss, it would be impossible for such a thin sheet to exhibit a complete Meissner effect up to this value. However, in a configuration like this, where, in the narrow pole gap of an iron magnet, a superconducting foil with an area larger than the pole piece is inserted, a modest Meissner current is apparantly sufficient to demagnetise the pole piece, keeping $B_1 - B_2 = 0$. (It cannot be decided from this experiment whether this means $B_1 = B_2 = 0$, a complete Meissner effect, or merely $B_1 = B_2 \neq 0$). It is clear from fig. 4 that in the second region, from Φ_M to Φ^1_{c2}(Φ^1_{c2} corresponding to a field value $B_1 = B_{c2}$ $\approx$ 3800 gauss) flux pinning plays a major role. If flux pinning is present in the sample, the specific resistance in the mixed state is not only a function of B but also of the current density. The ratio ρ_2/ρ_1, and therewith the ratio I_1/I_2, decreases from rotor I to rotor III and accounts for the inverse order of the $\overline{V}$ curves. The current density ratio for rotor III is even $I_2/I_1 =$ $= 3.65$, while $B_2/B_1 \approx 0.5$. This is evidently responsible for the negative

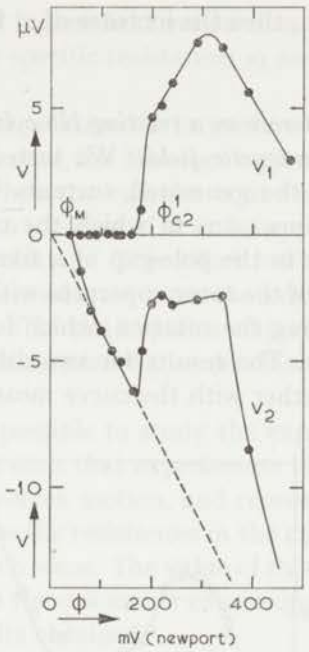

Fig. 11. The voltages V_1 and V_2 for rotor III in Nb, $v = 3.6 \times 10^{-3}$ m/s. (V_1 is measured at the front of the pole piece).

$\overline{V}$ in quite a large field region. The large current density ratio overcompensates the induction ratio, leading to $\rho_2 > \rho_1$. From fig. 11 we see, that, in a region at the front of the pole piece, $\rho_1 = 0$ where $\overline{V} < 0$ (fig. 4). (At the back of the pole piece V_1 is somewhat larger (fig. 6*a*) due to a small gradient in the vortex density, caused by the currents). The pictures for V_1, V_2 and $\overline{V}$ remain practically unchanged, qualitatively, for the whole velocity region from 0.7 m/s down to 3×10^{-3} m/s. This can be understood from the relation derived from eq. (12):

$$I_1\rho_1 + I_2\rho_2 = v(B_1 - B_2). \tag{13}$$

If for small v in a certain field region $\rho_1 = 0$, then the currents will stabilise on such a value that $I_2\rho_2 = v(B_1 - B_2)$. No matter how small v, the current density I_2 will be larger than a value $I_0(B_2)$, the value of I_2 at which pinning is first partly overcome. With increasing velocity I_2 will increase from I_0 rather slowly, as ρ_2 grows rapidly. Thus also I_1 will increase slowly with v. This can explain why ρ_1 stays zero for the whole range of velocities. In the region Φ^1_{c2} to Φ^2_{c2}, ρ_1 rapidly becomes equal to ρ_n, the specific resistance in the normal state, while ρ_2 decreases at first, due to the decreasing current densities and then grows to ρ_n also when B_2 approaches B_{c2}.

The results in tantalum (fig. 7) also show these three regions. First a

prolonged Meissner region, then the increase of ρ_1 from 0 to ρ_n and then the increase of ρ_2.

6' *Measurement of the forces on a rotating Nb-cylinder in a perpendicularly applied, inhomogeneous magnetic field.* We tested the conclusions drawn about the behaviour of the generated currents in the Nb-cylinder as a function of Φ with an apparatus in which the cylinder, suspended on a torsion wire, was rotated in the pole-gap of a fixed iron magnet, having a geometry similar to that of the rotor apparatus with rotor III. We measured the torsion angle $\Delta\alpha$ during the rotation, which is directly proportional to the force on the cylinder. The results for two different speeds of rotation are shown in fig. 12. together with the curve measured in the normal state

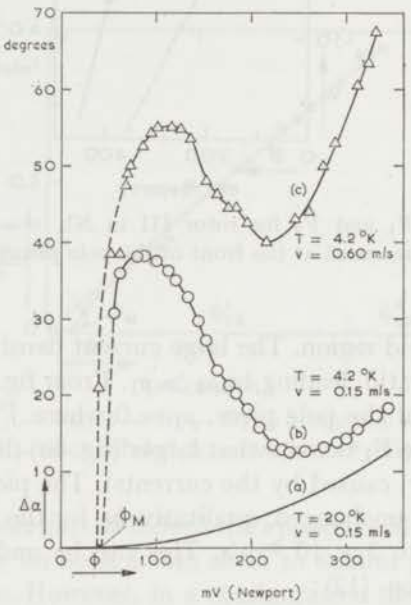

Fig. 12. The torsion angle $\Delta\alpha$ as a function of Φ.

at 20°K. For an idealised field pattern as sketched in fig. 3, the angle $\Delta\alpha$ is directly proportional to $i(B_1 - B_2)$, where i is the total current generated in the cylinder. As $B_1 - B_2$ increases linearly with Φ (fig. 10) and i is proportional to $B_1 - B_2$ at $T = 20°K$ (eqs. (5*a*) and (5*c*)) one expects a parabolic behaviour of $\Delta\alpha$ as a function of Φ, as is found indeed (fig. 12 curve a). The curves *b* and *c*, measured in the superconductive state, show the large Meissner region where $\Delta\alpha = 0$ and then the steep increase of $\Delta\alpha$ to a value only slightly dependent of the speed of rotation, in accordance with the conclusion that I_2 will stabilise in this field region on a current density roughly equal to $I_0(B_2)$.

The decrease of $\Delta\alpha$ for higher field values demonstrates the decrease of i due to an increase of the specific resistances ρ_1 and ρ_2 to the value ρ_n of the normal state.

It may be interesting to mention the large time-effects which occur during the sharp increase of $\Delta\alpha$ once the Meissner region is surpassed. If the field is increased above Φ_m when the cylinder is at rest, one notices, on setting the cylinder in motion, an increase of Φ and a corresponding sharp increase of $\Delta\alpha$ during several revolutions. This effect indicates that the flux, which can only enter the superconductor over the edge, needs time to find its equilibrium distribution. This also explains why very little hysteresis effects were observed when $\Delta\alpha$ is measured in a decreasing field.

It would of course be possible to study the experimental results in more detail, but since we have seen that experiments like this do not throw new light on the problem of vortex motion, and represent merely a complicated method to measure the specific resistances in the mixed state, we believe this would not make very much sense. The value of this work is determined more by the problems raised in the discussion concerning the vortex motion, than by the quantitative results obtained.

REFERENCES

1) De Gennes, P. G. and Matricon, J., Rev. mod. Phys. **36** (1964) 45.
2) Borcherds, P. H., Gough, C. E., Vinen, W. F. and Warren, A. C., Phil. Mag. **10** (1964) 349.
3) Volger, J., Staas, F. A. and Van Vijfeijken, A. G., Phys. Letters **9** (1964) 303.
4) Bardeen, J., Phys. Rev. Letters **13** (1964) 747.
5) Niessen, A. K. and Van Vijfeijken, A. G., Phys. Letters **16** (1965) 23.
6) Bardeen, J. and Stephen, M. J., Phys. Rev. **140** (1965) A1197.
7) Nozières, P. and Vinen, W. F., Phil. Mag. **14** (1966) 667.
8) Jones, R. G., Rhoderick, E. H. and Rose-Innes, A. C., Phys. Letters **15** (1965) 214.
9) Josephson, B. D., Phys. Letters **16** (1965) 242.
10) Casimir, H. B. G., Phys. Letters **17** (1965) 177.
11) Pearl, J., Phys. Rev. Letters **16** (1966) 99.
12) Park, J. G., Phys. Letters **20** (1966) 346.
13) Meincke, P. P. M., Phys. Rev. Letters **17** (1966) 390.
14) Kim, Y. B., Hempstead, C. F. and Strnad, A. D., Phys. Rev. **139** (1965) A1163.
15) Van Beelen, H., Arnold, Miss A. J. P. T., Sypkens, H. A., Van Braam Houckgeest, J. P., De Bruyn Ouboter, R., Beenakker, J. J. M. and Taconis, K. W., Commun. Kamerlingh Onnes Lab., Leiden No. 342*a*; Physica **31** (1965) 413.

THE MOTION OF VORTICES IN A TYPE II SUPERCONDUCTOR UNDER THE INFLUENCE OF A TRANSPORT CURRENT

Synopsis

The structure of the mixed state is discussed. The vortices are identified with the circulating supercurrents around the normal cores. When a conductor, carrying a current $\boldsymbol{i}_T$, is placed in a magnetic field $\boldsymbol{H}_a$, the force on the conductor per unit length will be given by: $\boldsymbol{F}_c = \mu_0 \boldsymbol{i}_T \times \boldsymbol{H}_a$, independent of the distribution of current and field within the conductor. The different mechanisms by which this force is transferred from the current carriers to the lattice are discussed, in the case of a normal metal, a type I superconductor, a type II superconductor with strong flux pinning and a pinning-free type II superconductor. It is shown that the observable voltage due to flux motion is given by: $V = -\int \boldsymbol{v}_\Phi \times \boldsymbol{B} \cdot d\boldsymbol{s}$, where $\boldsymbol{v}_\Phi$ is the velocity of the flux tubes and $\boldsymbol{B}$ the averaged induction in the sample. Assuming a uniform transport-current flow in stationary conditions in a pinning-free sample, the equation of motion for the vortices for $T \approx 0°K$ is found to be: $ne(\boldsymbol{v}_T - \boldsymbol{v}_\Phi) \times (\boldsymbol{\Phi}_0 + \boldsymbol{\Phi}_a) = 2\boldsymbol{f}$, where $ne\boldsymbol{v}_T$ represents the transport-current flow, Φ_0 is the unit of flux, Φ_a the flux contained by the core of the vortex and $\boldsymbol{f}$ the total friction with the lattice inside the core. The Hall angle and the specific resistance in the mixed state are derived from the equation of motion and show that a continuous transition to the normal state occurs at $H_a = H_{c_2}$. An increase of the Hall angle in the mixed state is predicted.

1. *Introduction.* The vortex motion in a pinning-free type II superconductor under influence of a transport current has been the subject of many recent studies[1–7]). Different results are obtained by different authors for the equation of motion of the vortices. These differences arise from different concepts with respect to both the driving force and the damping mechanism. Although there is agreement with respect to the observable voltage due to vortex motion, being $-\int \boldsymbol{v}_\Phi \times \boldsymbol{B} \cdot d\boldsymbol{s}$, there are differences in the mechanisms from which this result is obtained[8–13]). The aim of this chapter is to comment on these points. A picture, in which the vortex is a well-defined entity separated from the external field and the transport current, is introduced.

2. *The vortex structure in the mixed state.* When a type II superconductor is placed in a magnetic field exceeding a lower critical field, flux penetrates the specimen and the mixed state is attained[14]). This state is characterised by the existence of a vortex structure, *i.e.* an array of flux tubes embedded in superconducting material. The momentum of the superconducting electron pairs is quantised, in such a way that:

$$\oint \boldsymbol{p}_s \cdot \mathrm{d}\boldsymbol{s} = \oint (m\boldsymbol{v}_s + q\boldsymbol{A}) \cdot \mathrm{d}\boldsymbol{s} = \nu h \tag{2.1}$$

where $\nu = 1$ for any integration contour chosen around the quasi-normal core[15]) of a vortex and $\nu = 0$ if no vortex cores are embraced by the integration path (curl $\boldsymbol{p}_s = 0$). The vortices can be visualised having a quasi-normal core surrounded by superconducting material, in which supercurrents are maintained according to eq. (2.1). It follows from eq. (2.1) that the flux threading through one vortex cell equals:

$$\Phi_0 = \oint \boldsymbol{A} \cdot \mathrm{d}\boldsymbol{s} = h/q = h/2e \tag{2.2}$$

as between neighbouring vortices the velocity $\boldsymbol{v}_s$ goes to zero. The strength of the circulation current, or the total charge circulation around the vortex core, depends on the number of superconducting electron pairs participating in the motion. This arises from the fact that eq. (2.1) is a relation valid for the individual electron pairs and does not tell anything about the total current. The current strength is not only determined by the constants of the material, but also by the vortex density and consequently by the applied magnetic field strength. In the higher field region, where the vortices overlap more and more, the contribution of $\oint q\boldsymbol{A} \cdot \mathrm{d}\boldsymbol{s}$ will increase for any integration contour within the vortex cell, and $\oint m\boldsymbol{v}_s \cdot \mathrm{d}\boldsymbol{s}$ will decrease accordingly, in such a way that eq. (2.1) remains valid. The total field pattern in the specimen can be considered to be the sum of the applied field, corrected for the field associated with the shielding current around the sample, and the field pattern belonging to the circulation currents of the vortices[16]). For a thin foil in a perpendicularly applied field this means, for instance, that the vortices do not contribute to the total flux threading the sample, as the closed field patterns, belonging to the vortices, do not carry flux on a scale of the order of the thickness of the sheet. (The number of vortices, N, per unit area will, of course, still be given by $B = N\Phi_0$, where B is the macroscopic induction in the sample). When the applied field approaches the upper critical field H_{c_2}, the circulation currents, and with them the magnetic field modulation due to the vortex structure, will vanish gradually and a continuous transition to the normal state will occur.

In this picture one can define the vortex as an entity, which can move as a whole through the material when a "driving force" is exerted. We will identify the vortex with the circulation current. The magnetic field $\boldsymbol{b}_v$ of the vortex is merely the field generated by this current.

3. *The force on a type I superconductor carrying a current in an applied magnetic field.* A conductor, carrying a transport current $\boldsymbol{i}_T$ in a homogeneous applied magnetic field $\boldsymbol{H}_a$, will be subject to a force per unit length equal to:

$$\boldsymbol{F}_c = \mu_0 \boldsymbol{i}_T \times \boldsymbol{H}_a. \tag{3.1}$$

This force is unaffected by the current and field distribution within the conductor. How this force is transferred to the lattice will be discussed in the following paragraphs.

a. In a normal conductor the field component perpendicular to the current gives rise to a Hall field $\boldsymbol{E} = -\boldsymbol{\nabla}\varphi$ ($\partial \boldsymbol{A}/\partial t = 0$ in the stationary situation), which compensates the magnetic force on the moving current carriers q such that:

$$-q\boldsymbol{\nabla}\varphi + \mu_0 q \boldsymbol{v} \times \boldsymbol{H}_i = 0 \tag{3.2}$$

where $\boldsymbol{v}$ is the velocity of the current carriers and $\boldsymbol{H}_i$ the local field value in the sample. This electric field originates from a space-charge distribution in the sample. The magnetic force on the current carriers is transferred to the lattice by this space-charge field, as the electric force on the neutralising background equals:

$$\boldsymbol{F}_c = \iiint_\tau -\rho\boldsymbol{\nabla}\varphi \, d\tau = \iiint_\tau \rho(\boldsymbol{v} \times \boldsymbol{B}) \, d\tau = \mu_0 \boldsymbol{i}_T \times \boldsymbol{H}_a. \tag{3.3}$$

b. In a superconductor, from which the field is expelled except for a small surface layer, the penetration depth, the situation is different. The magnetic forces on the superconducting electrons are balanced by the forces of inertia[17]) as:

$$e\boldsymbol{v}_s \times \boldsymbol{B} = -\boldsymbol{v}_s \times \operatorname{curl} m\boldsymbol{v}_s \tag{3.4}$$

and no Hall field is measured in the superconductor. To fulfil the momentum balance it is necessary to assume the existence of surface forces, the London tension[17])[18]), through which the interaction with the lattice takes place. At the surface of the sample, where the current density $\boldsymbol{I}_s$ is parallel to the surface, the force density per unit area is:

$$F_s = \tfrac{1}{2}\Lambda I_s^2 = \tfrac{1}{2}(m/n_s e^2)\, n_s^2 e^2 v_s^2 = \tfrac{1}{2} n_s m v_s^2 \tag{3.5}$$

and points inwards into the material. In eq. (3.5) n_s represents the number of superconducting electrons per unit volume, m their mass and $\boldsymbol{v}_s$ their velocity. $\boldsymbol{I}_s$, and consequently $\boldsymbol{v}_s$, consists of a contribution $\boldsymbol{I}_T$ from the transport current and a contribution $\boldsymbol{I}_M$ from the Meissner current (responsible for the expulsion of $\boldsymbol{B}$). The current density is thus non-uniform along the surface. Integration of the London tension over the surface a of the superconductor leads to a force per unit length*):

$$\boldsymbol{F}_{s.c} = -\iint_a F_s \, d\boldsymbol{a} = -\iint_a \tfrac{1}{2} n_s m v_s^2 \, d\boldsymbol{a} = \mu_0 \boldsymbol{i}_T \times \boldsymbol{H}_a. \tag{3.6}$$

*) For a detailed calculation see appendix.

(This force can also be written as $\boldsymbol{F}_{s.c} = -\boldsymbol{i}_T \times 4\pi\boldsymbol{M}$, where $\boldsymbol{M}$ is the magnetisation per unit volume of the sample).

In order to obtain a physical picture of these surface forces we consider the equations of motion of the electron fluid. We will neglect spatial variations of n_s and n_n (the electron fluid is incompressible as has been shown by London (ref. 17 page 58), and the slight decrease of the internal order parameter $\psi^2 = n_s/n$ at the surface is neglected in this two fluid model) In a local theory the equation of motion for the superfluid can be written as:

$$n_s m(\partial \boldsymbol{v}_s/\partial t) + \boldsymbol{\nabla}\, \tfrac{1}{2} n_s m v_s^2 = n_s e\boldsymbol{E} - \boldsymbol{\nabla} P_s \tag{3.7}$$

where the pressure term $-\boldsymbol{\nabla} P_s$ arises from the relative motion of the superfluid with respect to the normal fluid. No gradients in the total chemical potential of the electron fluid are assumed to be present. We have used the basic property of the superfluid curl $\boldsymbol{p}_s = 0$, eq. (3.4), so that the Lorentz force $e\boldsymbol{v}_s \times \boldsymbol{B}$ does not appear in this equation. In stationary conditions $(\partial \boldsymbol{v}_s/\partial t) = 0$ so that eq. (3.7) reads as:

$$\boldsymbol{\nabla}\, \tfrac{1}{2} n_s m v_s^2 = n_s e\boldsymbol{E} - \boldsymbol{\nabla} P_s. \tag{3.8}$$

For the normal component we can write down:

$$0 = n_n e\boldsymbol{E} + \boldsymbol{\nabla} P_s \tag{3.9}$$

as we have assumed stationary flow with $\boldsymbol{v}_n = 0$. The total force on the lattice, exerted by the electric field, equals:

$$\boldsymbol{F}_{s.c} = -\iiint_{\tau} ne\boldsymbol{E}\, d\tau = \iiint_{\tau} -\boldsymbol{\nabla}\, \tfrac{1}{2} n_s m v_s^2\, d\tau = -\iint_{a} \tfrac{1}{2} n_s m v_s^2\, d\boldsymbol{a} = \mu_0 \boldsymbol{i}_T \times \boldsymbol{H}_a$$

and we have recovered the result of eq. (3.6). From eqs. (3.8) and (3.9) it follows that:

$$\boldsymbol{E} = (n_s/ne)\, \boldsymbol{\nabla}\, \tfrac{1}{2} m v_s^2 \tag{3.10}$$

and

$$\boldsymbol{\nabla} P_s \equiv n_s \nabla \mu_s^* = -n_s \boldsymbol{\nabla}\, \tfrac{1}{2}(n_n/n)\, m v_s^2. \tag{3.11}$$

Eq. (3.11) defines a new quantity μ_s^*, which we shall call the chemical potential of the superfluid component. From this equation it follows that for $\boldsymbol{v}_n = 0$ the result obtained by Landau for the chemical potential in helium II[19]) also holds for a superconductor as:

$$\mu_s^* = \mu - (n_n/n)\, \tfrac{1}{2} m v_s^2 = \mu + n_n(\partial\mu/\partial n_s). \tag{3.12}$$

It should be remarked that the integrated electric-field strength along a path in the sample is given by:

$$\int \boldsymbol{E} \cdot d\boldsymbol{s} = \int (n_s/ne)\, \boldsymbol{\nabla}(\tfrac{1}{2} m v_s^2) \cdot d\boldsymbol{s} \neq 0. \tag{3.13}$$

For a wire of circular cross section with radius R, carrying a transport current $\boldsymbol{i}_T$ in an applied magnetic field $\boldsymbol{H}_a$ perpendicular to the axis of the

wire, eq. (3.13) leads to a potential difference across the wire given by:

$$\Delta\varphi = (\mu_0/ne\pi R^2)\, \boldsymbol{i}_T \times \boldsymbol{H}_a \cdot \boldsymbol{s} \qquad (3.13')$$

where $\boldsymbol{s}$ is the path chosen through the superconductor (see appendix). That no Hall voltage is measured is due to a contact potential at the voltmeter connections. The chemical potential of the normal electrons follows from:

$$n_n \boldsymbol{\nabla}\mu_n^* \equiv \boldsymbol{\nabla}P_n = -\boldsymbol{\nabla}P_s = n_s \boldsymbol{\nabla}(n_n/n)\, \tfrac{1}{2}mv_s^2 \qquad (3.14)$$

so that:

$$\mu_n^* = \mu + (n_s/n)\, \tfrac{1}{2}mv_s^2 = \mu + n_s(\partial\mu/\partial n_n) \qquad (3.15)$$

with $n_s + n_n = n$ and $n_s\mu_s^* + n_n\mu_n^* = n\mu$ and $n_s(\partial\mu_s^*/\partial n_n) = n_n(\partial\mu_n^*/\partial n_s)$. The electrochemical potential $\mu_{ne}^* \equiv \mu_n^* + e\varphi$ is a constant throughout the superconductor, as can be seen from eq. (3.9). Continuity of this electrochemical potential at the voltmeter connections thus leads to a contact potential which exactly balances the electric-potential difference over the superconductor. One measures the electrochemical-potential difference across the sample rather than the electric-potential difference (see fig. 1).

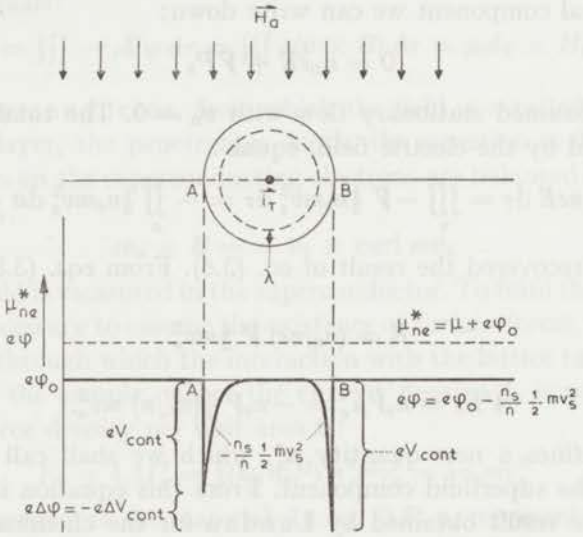

Fig. 1. Schematic diagram, showing the electrochemical potential μ_{ne}^* and the electric potential φ in a type I superconducting wire with voltmeter connections in the presence of a transport current and a perpendicularly applied magnetic field.

4. *The forces on a type II superconductor carrying a current in an applied magnetic field.* The force per unit length on a type II superconductor, carrying a current $\boldsymbol{i}_T$, which is brought in the mixed state by an applied magnetic field $\boldsymbol{H}_a$ will again be equal to:

$$\boldsymbol{F}_{s.c} = \mu_0 \boldsymbol{i}_T \times \boldsymbol{H}_a. \qquad (4.1)$$

This force, exerted by the magnet on the current carriers is transferred to the lattice partly by the mechanism discussed in section 3, due to a modest*) Meissner current around the sample responsible for the magnetization M**). The main part of the force, $\boldsymbol{i}_T \times \boldsymbol{B}$, with $\boldsymbol{B} = \mu_0 \boldsymbol{H}_a + 4\pi \boldsymbol{M}$ the magnetic induction in the sample ($B = N\Phi_0$), will be transferred to the lattice by a different mechanism, in which the vortices are involved.

a. We shall first consider the case in which the vortices are rigidly pinned to their positions in the lattice. This pinning can arise from irregularities in the lattice. In this case, where $\partial/\partial t = 0$, application of a local theory to the incompressible electron fluid leads to the equations of motion for the superfluid and normal fluid respectively, reading as:

$$\boldsymbol{\nabla} \tfrac{1}{2} m v_s^2 = e\boldsymbol{E} - \boldsymbol{\nabla} \mu_s^* \tag{4.2}$$

$$0 = e\boldsymbol{E} - \boldsymbol{\nabla} \mu_n^*. \tag{4.3}$$

Eq. (4.3) shows that the electrochemical potential μ_{ne}^* is again a constant throughout the sample and no voltage is observed (see fig. 2*a*). Using the expressions for μ_s^* and μ_n^* (eqs. 3.12 and 3.15), eqs. (4.2) and (4.3) become identical, reading as:

$$\boldsymbol{\nabla} \frac{n_s}{n} \tfrac{1}{2} m v_s^2 = e\boldsymbol{E} - \boldsymbol{\nabla} \mu. \tag{4.4}$$

The pinning of an individual vortex line can have several causes, from which we mention:

a) *surface pinning*. Local variations in the thickness of the sample causes pinning of vortex lines, due to the stretching energy of the vortex as a whole. This type of pinning also occurs when there are holes in the bulk of the material. The vortex will be pinned to those positions where its line energy is smallest.

b) *interaction with other vortices*. An individual vortex will be pinned to those positions where the total current flow throughout the vortex cell is zero. The transport-current flow is balanced by the sum of the circulation currents of the neighbouring vortices. It is clear that this type of pinning can only occur in combination with one of the other pinning mechanisms.

c) *pinning due to edge effects*. A barrier for the vortex may exist at the edges of the sample due to the local current distribution. (mirror force).

d) *pinning due to a gradient in the chemical potential* μ of the electron fluid. This gradient may arise from *e.g.* an applied temperature difference across the sample, but also from spatial variations in μ due to irregularities in the lattice.

*) modest compared to the case of a complete Meissner effect.

**) It seems plausible and we will assume that this contribution equals $-\boldsymbol{i}_T \times 4\pi \boldsymbol{M}$, as in the case of a type I superconductor.

We will consider case *d*) in somewhat more detail. We assume a uniform situation in the direction of the vortex axis, in such a way that each vortex is pinned down over its whole length by a gradient in the chemical potential μ. An electric field $\boldsymbol{E}$ will be built up in the stable situation in such a way that eq. (4.4) is fulfilled everywhere. The interaction with the lattice takes place through the electrochemical potential of the total electron fluid only; we thus obtain for the total force on the lattice:

$$\iiint_\tau n\nabla(\mu + e\varphi)\,\mathrm{d}\tau = \iiint_\tau n(\nabla\mu - e\boldsymbol{E})\,\mathrm{d}\tau = -\iiint_\tau n\nabla\frac{n_s}{n}\,\tfrac{1}{2}mv_s^2\,\mathrm{d}\tau \qquad (4.5)$$

which should be equal to $\boldsymbol{I}_T \times \boldsymbol{\Phi}_0$, in order that the total force on the lattice becomes:

$$\boldsymbol{F}_{s.c} = \boldsymbol{i}_T \times \boldsymbol{B} - \boldsymbol{i}_T \times 4\pi\boldsymbol{M} = \mu_0 \boldsymbol{i}_T \times \boldsymbol{H}_a. \qquad (4.6)$$

In fig. 2*a* the part of the electric potential which arises due to the presence of the vortices in a transport current, $e\varphi_1 = e\varphi - e\varphi_0 = -(n_s/n)\,\tfrac{1}{2}mv_s^2$ has been sketched schematically. The other part, $e\varphi_0$, balances the chemical potential μ in such a way that $\mu + e\varphi_0$ is constant throughout the sample.

b. When there are no inhomogeneities in the lattice there are no local electric fields to pin the vortices down and the vortices will start to move. Currents will be induced by the motion, from which the normal components in and around the vortex cores will encounter friction with the lattice. As

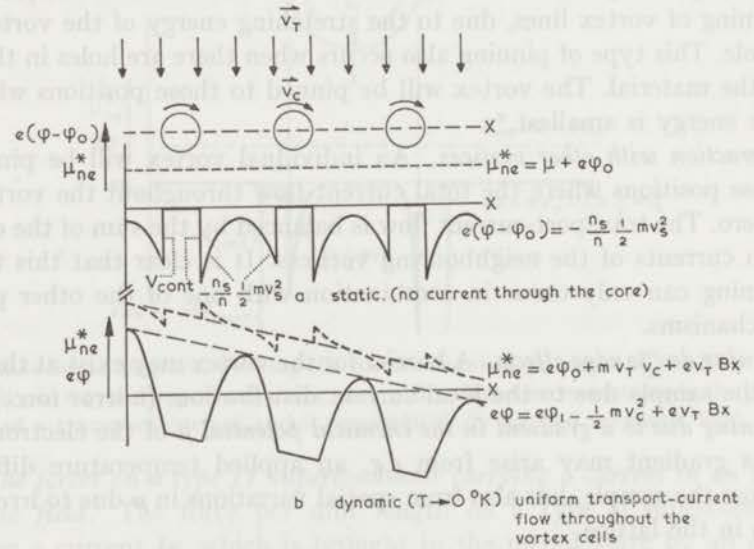

Fig. 2. Schematic diagram, showing the electrochemical potential μ^*_{ne} and the electric potential φ in a type II superconductor in the mixed state *a*) exhibiting complete flux pinning, *b*) without flux pinning.

will be shown in the next section there will arise a potential difference over the sample from the motion which results in a force on the lattice. Besides if there exists a contact potential V_{cont} on the interface at the core boundaries, the local electric fields in the vortex cells will contribute to the force on the lattice with

$$-\iint_{\text{core boundary}} neV_{\text{cont}}\,\mathrm{d}\boldsymbol{a}.$$

The friction forces, together with the electric field forces will add up to a total force on the lattice per vortex cell of unit length equal to $\boldsymbol{I}_{\text{T}} \times \boldsymbol{\Phi}_0$.

5. *The observable voltage due to flux motion.* As has been shown in chapter II[16]) the voltage due to vortex motion with a velocity $\boldsymbol{v}_\Phi$ equals:

$$V = -\int \boldsymbol{v}_\Phi \times \boldsymbol{B}\cdot\mathrm{d}\boldsymbol{s} = -\int N\boldsymbol{v}_\Phi \times \boldsymbol{\Phi}_0\cdot\mathrm{d}\boldsymbol{s}. \tag{5.1}$$

This result can also be obtained from the equations of motion for the superfluid and normal component of the electron fluid. These equations can be written as:

$$n_{\text{s}}m(\partial\boldsymbol{v}_{\text{s}}/\partial t) + \boldsymbol{\nabla}\tfrac{1}{2}n_{\text{s}}mv_{\text{s}}^2 = n_{\text{s}}e\boldsymbol{E} - \boldsymbol{\nabla}P_{\text{s}} \tag{5.2}$$

and

$$n_{\text{n}}m(\partial\boldsymbol{v}_{\text{n}}/\partial t) + \boldsymbol{\nabla}\tfrac{1}{2}n_{\text{n}}mv_{\text{n}}^2 - n_{\text{n}}m\boldsymbol{v}_{\text{n}} \times \operatorname{curl}\boldsymbol{v}_{\text{n}} = n_{\text{n}}e\boldsymbol{E} + n_{\text{n}}e\boldsymbol{v}_{\text{n}} \times (\boldsymbol{B} + \boldsymbol{b}_{\text{v}}) + \boldsymbol{\nabla}P_{\text{s}} - n_{\text{n}}m\boldsymbol{v}_{\text{n}}/\tau \tag{5.3}$$

in which $\boldsymbol{\nabla}P_{\text{s}} \equiv n_{\text{s}}\boldsymbol{\nabla}\mu_{\text{s}}^*$ again stands for the internal pressure gradient between the normal and superfluid component of the electronfluid. The vortices will again be considered to have a sharp boundary between the superfluid and the normal core. Spatial variations of the order parameter in the superfluid are neglected.

In stationary conditions we can replace:

$$(\partial\boldsymbol{v}_{\text{s}}/\partial t) = -(\boldsymbol{v}_\Phi\cdot\boldsymbol{\nabla})\,\boldsymbol{v}_{\text{s}} = -\boldsymbol{\nabla}(\boldsymbol{v}_\Phi\cdot\boldsymbol{v}_{\text{s}}) + \boldsymbol{v}_\Phi \times \operatorname{curl}\boldsymbol{v}_{\text{s}}. \tag{5.4}$$

By substituting eq. (5.4) into eq. (5.2) we obtain for the electric field $\boldsymbol{E}$:

$$n_{\text{s}}e\boldsymbol{E} = -\boldsymbol{\nabla}(n_{\text{s}}m\boldsymbol{v}_\Phi\cdot\boldsymbol{v}_{\text{s}} - \tfrac{1}{2}n_{\text{s}}mv_{\text{s}}^2 - P_{\text{s}}) + n\boldsymbol{v}_\Phi \times \operatorname{curl} m\boldsymbol{v}_{\text{s}}. \tag{5.5}$$

As for the superfluid:

$$0 = \operatorname{curl}\boldsymbol{p}_{\text{s}} = \operatorname{curl} m\boldsymbol{v}_{\text{s}} + e(\boldsymbol{B} + \boldsymbol{b}_{\text{v}}) \tag{5.6}$$

in which $\boldsymbol{B} = N\boldsymbol{\Phi}_0$ and $\boldsymbol{b}_{\text{v}}$ the magnetic field associated with the circulation currents, we obtain for $\boldsymbol{E}$:

$$e\boldsymbol{E} = -\boldsymbol{\nabla}(m\boldsymbol{v}_\Phi\cdot\boldsymbol{v}_{\text{s}} - \tfrac{1}{2}mv_{\text{s}}^2 - \mu_{\text{s}}^*) - e\boldsymbol{v}_\Phi \times \boldsymbol{B} - e\boldsymbol{v}_\Phi \times \boldsymbol{b}_{\text{v}}. \tag{5.7}$$

The voltage measured by a voltmeter connected between 1 and 2 (fig. 3)

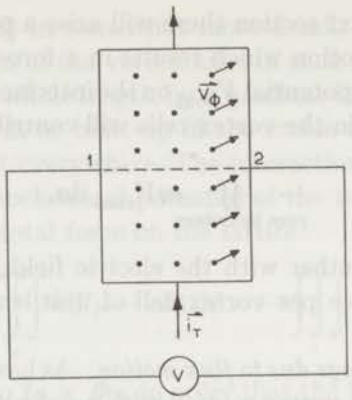

Fig. 3. The voltmeter arrangement.

across the sample will be given by (chapter II):

$$V_{21} = \int_1^2 \boldsymbol{E}\cdot \mathrm{d}\boldsymbol{s} + \dot{\Phi} \tag{5.8}$$

where the integral extends over a path through the superconductor and $\dot{\Phi}$ is the flux change within the closed contour formed by this path and the voltmeter. If we choose a path (I) completely through the superfluid, avoiding the vortex cores, we find for the measured voltage:

$$V = \int_1^2 -\boldsymbol{\nabla}(m\boldsymbol{v}_\Phi\cdot\boldsymbol{v}_\mathrm{s} - \tfrac{1}{2}mv_\mathrm{s}^2 - \mu_\mathrm{s}^*)/e\cdot \mathrm{d}\boldsymbol{s} - \int_1^2 \boldsymbol{v}_\Phi \times \boldsymbol{B}\cdot \mathrm{d}\boldsymbol{s} - \int_1^2 \boldsymbol{v}_\Phi \times \boldsymbol{b}_\mathrm{v}\cdot \mathrm{d}\boldsymbol{s} + \dot{\Phi}. \tag{5.9}$$

As only the vortex field $\boldsymbol{b}_\mathrm{v}$ is moving, $\dot{\Phi} = {}^2\!\int_1 \boldsymbol{v}_{\dot{\Phi}} \times \boldsymbol{b}_\mathrm{v}\cdot \mathrm{d}\boldsymbol{s}$. The gradient term in V drops out by integration, as its argument $(m\boldsymbol{v}_{\dot{\Phi}}\cdot\boldsymbol{v}_\mathrm{s} - \tfrac{1}{2}mv_\mathrm{s}^2 - \mu_\mathrm{s}^*)/e$ is constant at the boundaries between the vortex cells. (We deal with a situation in which the total transport current per vortex cell is assumed to be constant). We thus regain eq. (5.1) from eq. (5.9):

$$V = -\int_1^2 \boldsymbol{v}_\Phi \times \boldsymbol{B}\cdot \mathrm{d}\boldsymbol{s} = -\int_1^2 N\boldsymbol{v}_\Phi \times \boldsymbol{\Phi}_0\cdot \mathrm{d}\boldsymbol{s}.$$

It should be remarked that in this case there is no contact potential at the voltmeter connections which compensates this voltage*). The electrochemical potential of the normal electrons is not a constant in the sample, but contains a term corresponding with the potential difference $(-\boldsymbol{v}_\Phi \times \boldsymbol{B})\cdot\boldsymbol{s}$. As the internal pressure P_s is constant at the boundaries between the vortex cells, it cannot compensate for this potential difference (see fig. 2*b*).

*) There is a small contact potential at the voltmeter connections due to a modest Meissner current around the sample (See section 3).

We believe that the discussion given above is a more thorough proof of the result given by eq. (5.1) than has been given so far[8–13]).

6. *The equation of motion for the vortices.* We will, for simplicity, neglect the influence of the normal component of the electron fluid outside the vortex core and derive the equation of motion for $T \approx 0°\mathrm{K}$. The total force on the lattice will arise from the electric fields and the friction, as was mentioned in section 4*b*. If we *assume* uniform transport-current flow throughout the vortex cells, in accordance with the proposal made by Kim, Hempstead and Strnad[20]) in order to interpret their experimental results and with the theoretical derivation of Bardeen and Stephen[6]) we can write eq. (5.8) (taking $n_n = 0$ and thus $\mu_s^* = 0$) in the form:

$$\boldsymbol{E}_{\mathrm{out}} = -\boldsymbol{\nabla}(m\boldsymbol{v}_\Phi \cdot \boldsymbol{v}_c - \tfrac{1}{2}mv_s^2)/e - \boldsymbol{v}_\Phi \times \boldsymbol{B} - \boldsymbol{v}_\Phi \times \boldsymbol{b}_v = -\boldsymbol{\nabla}\varphi_{\mathrm{out}} - \boldsymbol{v}_\Phi \times \times (\boldsymbol{b}_v + \boldsymbol{B}) \qquad (6.1)$$

and

$$\boldsymbol{E}_{\mathrm{in}} = -\boldsymbol{\nabla}\varphi_{\mathrm{in}} - \boldsymbol{v}_\Phi \times \boldsymbol{B} - \boldsymbol{v}_\Phi \times \boldsymbol{b}_v. \qquad (6.2)$$

$\boldsymbol{E}_{\mathrm{out}}$ and $\boldsymbol{E}_{\mathrm{in}}$ represent the field outside and inside the core respectively. We then obtain for the total force exerted on the lattice by the electric fields:

$$\boldsymbol{F}_E = -\iiint_{\text{vortex cell}} ne\boldsymbol{E}\,\mathrm{d}\tau = ne\iiint_\tau \boldsymbol{\nabla}\varphi_{\mathrm{out}}\,\mathrm{d}\tau + ne\iiint_\tau \boldsymbol{\nabla}\varphi_{\mathrm{in}}\,\mathrm{d}\tau + ne\boldsymbol{v}_\Phi \times \boldsymbol{\Phi}_0. \qquad (6.3)$$

When $\mathrm{d}\boldsymbol{a}$ represents a surface element of the interface between the superfluid and the normal core, pointing into the core, we can write eq. (6.3) as:

$$\boldsymbol{F}_E = ne\iint_a (\varphi_{\mathrm{out}} - \varphi_{\mathrm{in}})\,\mathrm{d}\boldsymbol{a} + ne\boldsymbol{v}_\Phi \times \boldsymbol{\Phi}_0 \equiv ne\iint_a V_{\mathrm{cont}}\,\mathrm{d}\boldsymbol{a} + ne\boldsymbol{v}_\Phi \times \boldsymbol{\Phi}_0. \qquad (6.4)$$

The friction force inside the core is simply given by:

$$\boldsymbol{f} = n(m\boldsymbol{v}_T/\tau)\,\pi a^2 \qquad (6.5)$$

in which τ stands for the electron-lattice collision time and a is the core radius.

There occurs also friction with the lattice at the core boundary, where the superconducting electrons are excited to the normal state and subsequently lose their mechanical circulation momentum $m\boldsymbol{v}_c$ to the lattice[7]). At the rear side of the vortex core the inverse process takes place and momentum from opposite sign has to be supplied by the lattice. As per second, in an area $\mathrm{d}\boldsymbol{a}$ of the interface, $n(\boldsymbol{v}_\Phi - \boldsymbol{v}_T)\cdot\mathrm{d}\boldsymbol{a}$ electrons lose their momentum $m\boldsymbol{v}_c$, we obtain for the total momentum loss to the lattice:

$$-(\partial\boldsymbol{P}/\partial t)_{\mathrm{boundary}} = \iint_a n(\boldsymbol{v}_\Phi - \boldsymbol{v}_T)\cdot m\boldsymbol{v}_c\,\mathrm{d}\boldsymbol{a} = \tfrac{1}{2}ne(\boldsymbol{v}_T - \boldsymbol{v}_\Phi) \times (\boldsymbol{\Phi}_0 - \boldsymbol{\Phi}_a)\,^*) \qquad (6.6)$$

*) The factor $\frac{1}{2}$ arises from the uniform transport current outside as well as inside the core.

where $\Phi_a = \Phi_0 - \oint_{c,b} (m/e)\, \boldsymbol{v}_c \cdot d\boldsymbol{s}$ represents the total flux contained by the core. The total force on the lattice equals:

$$\boldsymbol{F}_{s.c} = \boldsymbol{F}_E + \boldsymbol{f} - (\partial \boldsymbol{P}/\partial t)_b$$

which becomes, using eqs. (6.4), (6.5) and (6.6):

$$\boldsymbol{F}_{s.c} = ne \iint_a V_{cont}\, d\boldsymbol{a} + ne\boldsymbol{v}_\Phi \times \boldsymbol{\Phi}_0 + \tfrac{1}{2} ne(\boldsymbol{v}_T - \boldsymbol{v}_\Phi) \times (\boldsymbol{\Phi}_0 - \boldsymbol{\Phi}_a) + \boldsymbol{f}. \quad (6.7)$$

By equating $\boldsymbol{F}_{s.c}$ to $\boldsymbol{I}_T \times \boldsymbol{\Phi}_0$ we obtain for the equation of motion of the vortices:

$$\tfrac{1}{2} ne(\boldsymbol{v}_T - \boldsymbol{v}_\Phi) \times (\boldsymbol{\Phi}_0 + \boldsymbol{\Phi}_a) - ne \iint_a V_{cont}\, d\boldsymbol{a} = \boldsymbol{f}. \quad (6.8)$$

It is easily shown that this result is consistent with the assumption that the transport current flows uniformly through the core of the vortex. The electric field inside the core must be given by:

$$\boldsymbol{E}_{in} = -\boldsymbol{v}_T \times \boldsymbol{B}_c + m\boldsymbol{v}_T/e\tau \quad (6.9)$$

where $\boldsymbol{B}_c = \boldsymbol{B} + \boldsymbol{b}_v$, the total magnetic field inside the core. From eq. (6.2) and the definition of V_{cont} given in eq. (6.4) we obtain:

$$ne \iiint_{core} \boldsymbol{E}_{in}\, d\tau = ne \iiint -\boldsymbol{V}\varphi_{in}\, d\tau - ne\boldsymbol{v}_\Phi \times \boldsymbol{\Phi}_a =$$

$$ne \iint_a \varphi_{in}\, d\boldsymbol{a} - ne\boldsymbol{v}_\Phi \times \boldsymbol{\Phi}_a =$$

$$ne \iint_a \varphi_{out}\, d\boldsymbol{a} - ne \iint_a V_{cont}\, d\boldsymbol{a} - ne\boldsymbol{v}_\Phi \times \boldsymbol{\Phi}_a$$

By substituting for $ne \iint_a V_{cont}\, d\boldsymbol{a}$ from eq. (6.8) and using the expression for φ_{out} as given in eq. (6.1) we obtain:

$$ne \iiint \boldsymbol{E}_{in}\, d\tau = ne\, \boldsymbol{E}_{in} \pi a^2 = -ne\boldsymbol{v}_T \times \boldsymbol{\Phi}_a + \boldsymbol{f}$$

as was required by eq. (6.9).

It is clear from eq. (6.8) that the motion of the vortices is controlled by the contact potential. An independent expression for the contact potential is needed in order to solve the problem. In the theories of Van Vijfeijken and Niessen[5]) and of Bardeen and Stephen[6]) such an expression is obtained by requiring that the electro-chemical potential is continuous at the core boundary. In the paper of Nozières and Vinen[7]) it is argued that such an assumption is not very plausible. They show that the absence of a contact potential leads to results which give the correct behaviour in the very pure limit ($\tau \to \infty$). We will also assume that:

$$ne \iint_a V_{cont}\, d\boldsymbol{a} = 0. \quad (6.10)$$

This seems to be a very plausible assumption, since it implies a discontinuity in the electrochemical potential of the normal electrons in a frame

moving with the vortex, $\overline{\Delta\mu^*_{ne}}$, given by:

$$n \iint_a \overline{\Delta\mu^*_{ne}}\, \mathrm{d}\boldsymbol{a} = \iint_a \tfrac{1}{2} nm(\boldsymbol{v}_s - \boldsymbol{v}_\phi)^2\, \mathrm{d}\boldsymbol{a} = -\tfrac{1}{2} ne(\boldsymbol{v}_T - \boldsymbol{v}_\phi) \times (\boldsymbol{\Phi}_0 - \boldsymbol{\Phi}_a) \quad (6.11)$$

This shows that the total friction force on the electrons at the core boundary, $(\partial \boldsymbol{P}/\partial t)_b$, is balanced by a change in the electrochemical potential in the moving frame, as from eqs. (6.6) and (6.11) it follows that:

$$(\partial \boldsymbol{P}/\partial t)_b - n \iint_a \overline{\Delta\mu^*_{ne}}\, \mathrm{d}\boldsymbol{a} = 0. \quad (6.12)$$

From eqs. (6.8) and (6.10) we thus arrive at the equation of motion, derived for $T \approx 0°\mathrm{K}$, reading as

$$\tfrac{1}{2} ne(\boldsymbol{v}_T - \boldsymbol{v}_\phi) \times (\boldsymbol{\Phi}_0 + \boldsymbol{\Phi}_a) = \boldsymbol{f} = n(m\boldsymbol{v}_T/\tau)\, \pi a^2. \quad (6.13)$$

It should be remarked that one can consider eq. (6.12) as the more fundamental relation, determining the boundary condition at the interface between the superfluid and the normal cores. If we allow the presence of a contact potential at the interface, we can write for the jump in the electrochemical potential at the core boundary in a frame moving with the vortex:

$$n \iint_a \overline{\Delta\mu^*_{ne}}\, \mathrm{d}\boldsymbol{a} = -\tfrac{1}{2} ne(\boldsymbol{v}_T - \boldsymbol{v}_\phi) \times (\boldsymbol{\Phi}_0 - \boldsymbol{\Phi}_a) + ne \iint_a V_{cont}\, \mathrm{d}\boldsymbol{a} \quad (6.14)$$

The term $(\partial \boldsymbol{P}/\partial t)_b$ in eq. (6.12) can then again be regarded as the friction force on the electrons, exerted by the lattice at the core boundary. This friction force, however, may differ from the force given in eq. (6.6) due to an additional damping mechanism, *e.g.* a mechanism as proposed by Tinkham[21]).

If we write down a more general equation of motion for the vortices, by leaving out the substitution of eq. (6.6), we arrive at:

$$ne\boldsymbol{v}_\phi \times \boldsymbol{\Phi}_0 + ne \iint_a V_{cont}\, \mathrm{d}\boldsymbol{a} - (\partial \boldsymbol{P}/\partial t)_b + \boldsymbol{f} = ne\boldsymbol{v}_T \times \boldsymbol{\Phi}_0 \quad (6.15)$$

Combining eqs. (6.12), (6.14) and (6.15) leads to an equation of motion:

$$\tfrac{1}{2} ne(\boldsymbol{v}_T - \boldsymbol{v}_\phi) \times (\boldsymbol{\Phi}_0 + \boldsymbol{\Phi}_a) = \boldsymbol{f}$$

which is identical with eq. (6.13). The equation of motion thus appears to be independent of the exact form of the friction at the core boundary. A contact potential will exist in stationary conditions such that eq. (6.13) remains essentially unchanged. However, the requirement of uniform transport current flow is only fulfilled when the total friction at the core boundary is as given by eq. (6.6) and thus $ne \iint_a V_{cont}\, \mathrm{d}\boldsymbol{a} = 0$.

7. *The specific resistance and the Hall angle in the mixed state.* From eq. (6.13) the vortex velocity components parallel ($v_\phi^{//}$) and perpendicular ($v_\phi^{\perp}$)

to the current follow directly:

$$v_\Phi^{//} = v_T \tag{7.1}$$

and

$$v_\Phi^{\perp} = 2(m/e\tau)(\pi a^2/(\Phi_0 + \Phi_a))\, v_T. \tag{7.2}$$

The vortex thus moves along with the current in the very pure limit ($\tau \to \infty$). Using eqs. (5.1) and (7.1) we obtain for the Hall voltage:

$$E^{\perp} = v_T B. \tag{7.3}$$

It is clear from eq. (7.3) that the Hall voltage approaches that of the normal state continuously when $H_a \to H_{c_2}$. The longitudinal voltage follows from eqs. (5.1) and (7.2):

$$E^{//} = 2(m/ne^2\tau)(a^2/d^2)(\Phi_0/(\Phi_0 + \Phi_a))\, I_T = 2(a^2/d^2)(\Phi_0/(\Phi_0 + \Phi_a))\, \rho_n I_T \tag{7.4}$$

in which d is the radius of the vortex cells and $\rho_n = (m/ne^2\tau)$, the specific resistance in the normal state. From eq. (7.4) the specific resistance in the mixed state is found to be:

$$\rho_{eff} = 2(a^2/d^2)(\Phi_0/(\Phi_0 + \Phi_a))\, \rho_n. \tag{7.5}$$

For materials in which $\lambda \gg \xi$ (ξ the coherence length) this corresponds to the phenomenological relation found by Kim *e.a.*[20]) in the low field region where $\Phi_a \ll \Phi_0$:

$$\rho_{eff} = 2(a^2/d^2)\, \rho_n \tag{7.6}$$

In the high field region, when H_a approaches H_{c_2}, Φ_a will approach Φ_0 and thus $\rho_{eff} \to \rho_n$.

For the Hall angle we find from eqs. (7.3) and (7.4):

$$\operatorname{tg} \theta_m \equiv E^{\perp}/E^{//} = (e\tau/m)(\Phi_0 + \Phi_a)/2\pi a^2. \tag{7.7}$$

In order to compare this result with the experiments we need an expression for the core radius, a, and the field inside the core, B_c. If we use for a the interpolation argument, suggested by Bardeen and Stephen[6]) taking:

$$(\Phi_0/2\pi a^2) = \mu_0(H_{c_2} - \tfrac{1}{2}H_a) \tag{7.8}$$

we obtain for the Hall angle:

$$\operatorname{tg} \theta_m = (e\tau/m)(\mu_0 H_{c_2} - \mu_0 H_a/2 + B_c/2). \tag{7.9}$$

Relation (7.9) shows that the Hall angle increases on entering the mixed state, as B_c will decrease only slowly with decreasing H_a. This increase is in qualitative agreement with the measured Hall angle in Nb–Ta samples[22]) but does not explain the current-dependent Hall angle found in a very pure Nb sample[23]).

8. *Discussion.* The equation of motion for a vortex in a type II superconductor, being driven by a transport current, has been derived for a rather crude model. We mention the following assumptions which are made:

1. the problem is treated as a two-dimensional problem, in the sense that possible corrections, due to the finite length of the vortices are not taken into account. It is assumed that the vortices are not bent due to the motion. As has been shown by Pearl[24]), the vortex structure is considerably different at the surface of the superconductor, over a depth of the order of the penetration depth. In specimens, which are thick compared to the penetration depth, corrections, due to surface effects, on the equation of motion may be expected to be small.

2. use is made of a local theory. The vortex structure is simplified strongly by taking a model in which the normal vortex core has a sharp boundary, outside which the superfluid order parameter immediately attains its equilibrium value. The depairing region, just outside the normal vortex core, is thus taken to be localised on the interface between the core and the superfluid. The Cooper pairs depair on the interface where they loose their mechanical circulation momentum to the lattice. It seems plausible, however, that this simplified model bears the same essential features as a more refined model.

3. the equation of motion has been derived only for $T \to 0°\mathrm{K}$, as the friction outside the vortex cores of the normal electrons with the lattice has been neglected entirely. An extension to higher temperatures has not been made.

It should be remarked that it has proved not to be necessary to introduce the "force on a vortex". The definition of such a force, exerted by the transport current on the vortices, seems to us to have a somewhat arbitrary nature. It seems not possible to divide the superfluid in a part belonging to the vortex and one belonging to the transport current, since both are carried by the same fluid elements. Still one can read the equation of motion (eq. (6.13)), which is essentially a force-balance equation, as:

$$\boldsymbol{F}_{\mathrm{M}} = ne(\boldsymbol{v}_{\mathrm{T}} - \boldsymbol{v}_{\Phi}) \times \boldsymbol{\Phi}_0 = \tfrac{1}{2}ne(\boldsymbol{v}_{\mathrm{T}} - \boldsymbol{v}_{\Phi}) \times (\boldsymbol{\Phi}_0 - \boldsymbol{\Phi}_{\mathrm{a}}) + \boldsymbol{f}$$

or, if one likes, as:

$$\boldsymbol{F}_{\mathrm{L}} = ne\boldsymbol{v}_{\mathrm{T}} \times \boldsymbol{\Phi}_0 = ne\boldsymbol{v}_{\Phi} \times \boldsymbol{\Phi}_0 + \tfrac{1}{2}ne(\boldsymbol{v}_{\mathrm{T}} - \boldsymbol{v}_{\Phi}) \times (\boldsymbol{\Phi}_0 - \boldsymbol{\Phi}_{\mathrm{a}}) + \boldsymbol{f}$$

Written in this way one can consider $\boldsymbol{F}_{\mathrm{M}}$ respectively $\boldsymbol{F}_{\mathrm{L}}$ as the "driving force" on the vortex which is balanced by the reaction forces due to the motion.

Or, to say with Nozières and Vinen[7]); it is merely a question of semantics, how one presents the equation of motion.

4. the transport current in the pinning-free case is assumed to be uniform, throughout the vortex cells. This leads to the choice of such a contact potential at the interface that $ne \iint_a V_{\mathrm{cont}}\, \mathrm{d}\boldsymbol{a} = 0$, if one assumes that the friction force with the lattice at the interface between core and superfluid, must be equal to the surface integral of the electrochemical potential of the normal component of the superfluid in a frame moving with the vortex.

In order to compare with experiments it is necessary to justify these assumptions. On the other hand, the experimental results may be influenced by flux pinning. The current dependent Hall angle found in very pure Nb[23]) points strongly into the direction of flux pinning, while the results on Nb–Ta[22]) are obtained by using a calculation technique with which the influence of guided motion is eliminated.

APPENDIX

From curl $\boldsymbol{p}_s = 0$ it follows immediately that the current distribution in a type I superconductor is governed by the differential equation:

$$\Delta \boldsymbol{I} = \boldsymbol{I}/\lambda^2 \tag{A.1}$$

in which $\lambda = (m/\mu_0 n e^2)^{\frac{1}{2}} = (\Lambda\mu_0)^{\frac{1}{2}}$, the penetration depth. From eq. (A.1) it follows that the distribution of a transport current i_T in the z direction in a circular cylinder of radius R is given by:

$$I_{zT} = \frac{i_T}{2\pi\lambda R}\, j\, \frac{J_0(jr/\lambda)}{J_1(jR/\lambda)} \tag{A.2}$$

in which $j = (-1)^{\frac{1}{2}}$ and J_0 and J_1 are Bessel-functions[18]).
If the cylinder is placed in a homogeneous magnetic field H_a in the positive x direction, a shielding current is induced so that the magnetic field is expelled from the interior of the cylinder. Solving eq. (A.1) in this case leads to a shielding current distribution given by:

$$I_{zs} = \frac{2H_a}{\lambda}\, j\, \frac{J_1(jr/\lambda)}{J_0(jR/\lambda)} \sin\theta. \tag{A.3}$$

For a cylinder carrying a transport current i_T which is placed in a magnetic field H_a we thus obtain by superposition of I_{zT} and I_{zs} for the force density at the surface:

$$F_s = \tfrac{1}{2}\Lambda I_s^2 = \tfrac{1}{2}\Lambda\left(I_{zT}^2 + I_{zs}^2 - 2\,\frac{i_T H_a}{\pi\lambda^2 R}\sin\theta\right). \tag{A.4}$$

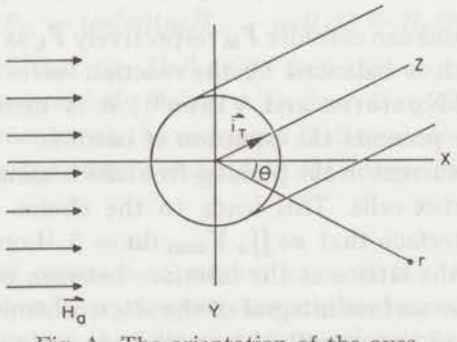

Fig. A. The orientation of the axes.

From eq. (A.4) we derive for the total pressure in the y direction:

$$\boldsymbol{F}_{\mathrm{s.c}} = -\boldsymbol{e}_y \int_0^{2\pi} F_{\mathrm{s}} \sin\theta \, R \, \mathrm{d}\theta = \mu_0 \boldsymbol{i}_{\mathrm{T}} \times \boldsymbol{H}_{\mathrm{a}} \tag{A.5}$$

which is the result used in eq. (3.6).
For the line integral of the electric field strength $\boldsymbol{E}$ we obtain:

$$\int_s \boldsymbol{E}\cdot\mathrm{d}\boldsymbol{s} = (ne)^{-1} \int_s \boldsymbol{\nabla}(\tfrac{1}{2} n_{\mathrm{s}} m v_{\mathrm{s}}^2)\cdot\mathrm{d}\boldsymbol{s} = (ne)^{-1} \int_s \boldsymbol{\nabla}(\tfrac{1}{2}\Lambda I_{\mathrm{s}}^2)\cdot\mathrm{d}\boldsymbol{s} = (ne)^{-1}\Lambda\tfrac{1}{2}\Lambda I_{\mathrm{s}}^2. \tag{A.6}$$

By combining eqs. (A.2), (A.3) and (A.4) with eq. (A.6) we obtain for the potential difference between two points, lying diametrically on the surface of the cylinder:

$$-\Delta\varphi = \int_s \boldsymbol{E}\cdot\mathrm{d}\boldsymbol{s} = \frac{\mu_0 i_{\mathrm{T}} H_{\mathrm{a}} R}{ne\pi R^2} (\sin\theta_2 - \sin\theta_1) = \frac{\mu_0}{ne\pi R^2} \boldsymbol{i}_{\mathrm{T}} \times \boldsymbol{H}_{\mathrm{a}}\cdot\boldsymbol{s} \tag{A.7}$$

as was given in eq. (3.13′).

REFERENCES

1) De Gennes, P. G. and Matricon, J., Rev. mod. Phys. **36** (1964) 65.
2) Volger, J., Staas, F. A. and Van Vijfeijken, A. G., Phys. Letters **9** (1964) 303.
3) Bardeen, J., Phys. Rev. Letters **13** (1964) 747.
4) Niessen, A. K. and Van Vijfeijken, A. G., Phys. Letters **16** (1965) 23.
5) Van Vijfeijken, A. G. and Niessen, A. K., Philips Research Reports **20** (1965) 505.
6) Bardeen, J. and Stephen, M. J., Phys. Rev. **140** (1965) A1197.
7) Nozières, P. and Vinen, W. F., Phil. Mag. **14** (1966) 667.
8) Jones, R. G., Rhoderick, E. H. and Rose-Innes, A. C., Phys. Letters **15** (1965) 214.
9) Josephson, B. D., Phys. Letters **16** (1965) 242.
10) Casimir, H. B. G., Phys. Letters **17** (1965) 177.
11) Pearl, J., Phys. Rev. Letters **16** (1966) 99.
12) Park, J. G., Phys. Letters **20** (1966) 346.
13) Meincke, P. P. M., Phys. Rev. Letters **17** (1966) 390.
14) Abrikosov, A. A., Sov. Phys. JETP **5** (1957) 1174.
15) Caroli, C., De Gennes, P. G. and Matricon, J., Phys. Letters **9** (1964) 307.
16) Van Beelen, H., Van Braam Houckgeest, J. P., De Bruyn Ouboter, R. and Taconis, K. W., Commun. Kamerlingh Onnes Lab., Leiden No. 358*a*; Physica **36** (1967) 107.
17) London, F., Superfluids I (Dover Publ. Inc., New York, 1960).
18) Von Laue, M., Theorie der Supraleitung (Springer Verlag, Berlin, Göttingen, 1949).
19) Landau, L. D., J. Phys. U.S.S.R. **5** (1941) 71, eq. (7.8).
Landau, L. D. and Lifshitz, E. M., Fluid Mechanics (Pergamon Press, Oxford 1963) p. 514.
20) Kim, Y. B., Hempstead, C. F. and Strnad, A. D., Phys. Rev. **139** (1965) A1163.
21) Tinkham, M., Phys. Rev. Letters **13** (1964) 804.
22) Niessen, A. K. and Staas, F. A., Phys. Letters **15** (1965) 26.
Niessen, A. K., Staas, F. A. and Weijsenfeld, C. H., Contributed paper to the conference on transport properties in superconductors, March 1967, Canterbury.
23) Reed, W. A., Fawcett, E. and Kim, Y. B., Phys. Rev. Letters **14** (1965) 790.
24) Pearl, J., J. appl. Phys. **37** (1966) 4139.

CHAPTER IV

SOME MEASUREMENTS ON THE EFFECTIVE RESISTANCE AND THE HALL ANGLE IN TYPE II SUPERCONDUCTORS

Synopsis

Resistivity and transverse-voltage measurements on In–40 at% Pb and on Nb samples are reported. A model for flux pinning, which accounts for the straight character of the voltage *versus* current characteristics is presented and compared with the results. The influence of the surface layer in the Nb samples has been studied and it is found that in the mixed-state region a surface layer is ineffective for the current-carrying capacity of these samples. The measured transverse voltages, which can be divided into even and odd components, are discussed. It is shown that a slight gradient in the applied magnetic field gives rise to rather large even transverse voltages, when the usual potentiometer arrangement is used. The accuracy obtained for the uneven transverse-voltage component is rather badly influenced by this effect. The calculated Hall angles in the In_{60}–Pb_{40} samples show an increase in the mixed state. The Nb samples show a change of sign of the Hall angle in the mixed state, which is suggested to be due to a change of mobility of the current carriers within the small cores of the vortices.

1. *Introduction.* A type II superconductor, which is brought into the mixed state by an applied magnetic field, exhibits resistance as well as a Hall effect in the presence of a transport current. These phenomena are generally understood to be due to the motion of the vortex pattern, which is driven by the transport current. The generated voltage, due to this motion, can be expressed in the vortex velocity $\boldsymbol{v}_\Phi$ as:

$$\boldsymbol{E} = -\boldsymbol{v}_\Phi \times \boldsymbol{B} = -\boldsymbol{v}_\Phi \times N\boldsymbol{\Phi}_0$$

in which $\boldsymbol{B} = N\boldsymbol{\Phi}_0$ stands for the magnetic induction in the sample and N is the number of vortices of unit fluxoid $\Phi_0 = h/2e$ per unit area. All the existing theories[1–4]) predict $\boldsymbol{v}_\Phi$ to have a component parallel as well as perpendicular to the transport current, thus giving rise to a transverse and a longitudinal voltage. The magnitude of the $\boldsymbol{v}_\Phi$-components are slightly

different from one theory to another. This gives rise to differences in the expected voltages, resulting in a considerable difference in the Hall angle, which is predicted to be either equal to the extrapolated value of the normal state[1]), or slightly larger[2]) or constant in the mixed state at a value equal to the Hall angle in the normal state for an applied field $H_a = H_{c_2}$[3]). In chapter III[4]) we calculated an increase of the Hall angle in the mixed state. It has not been possible yet to decide unambiguously from experiment between these theories, as the measured results are greatly influenced by vortex pinning. The vortices usually cannot move freely through the sample but are kept or guided by unavoidable irregularities in the lattice of the superconductor. These effects are dominant in most cases and make an unambiguous choice between the theories so far not possible. The experimental results on the Hall angle in Nb–Ta alloys[5]) show that an increase occurs on entering the mixed state, in good qualitative agreement with the predictions in ref. 4. The Hall angle is calculated with a technique in which the influence of guided motion of vortices is eliminated[6]). The Hall angle measurements on a very pure niobium sample[7]) show a current-dependent result in the mixed state, and the Hall angle decreases on entering the mixed state. This current dependence of the Hall angle is not predicted by any of the theories and points strongly into the direction of flux pinning.

In this chapter we will report on resistivity and Hall angle measurements in "pinning" type II superconductors and discuss some of the effects caused by pinning.

2. *The experiment.* The measurements on the resistivity and Hall angle are carried out in the standard way. We used specimens which were cut of a big foil in the shape sketched in fig. 1. The voltmeter is connected to

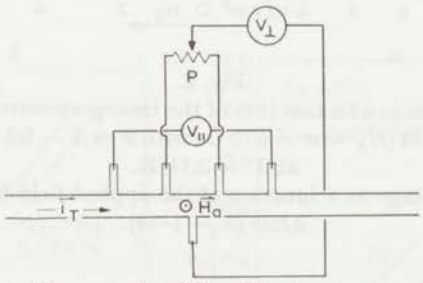

Fig. 1. The sample with voltmeter arrangement.

narrow side strips, narrow so that the disturbance of the transport current distribution is small. The transverse voltage is measured by using a potentiometer arrangement outside the cryostat with which the component of the longitudinal voltage can be compensated. The potentiometer is adjusted in such a way that in high magnetic fields ($H_a \approx 2H_{c_2}$) the transverse

voltage is symmetric with respect to zero upon reversing the field. The voltages are measured with a Keithley micro-voltmeter type 150A, from which the output is fed to the y axis of a Moseley x–y recorder, type 135AM. A signal, proportional to either the current through the Nb–Zr superconducting magnet or to the transport current is fed to the x axis of the recorder.

Some transverse-voltage measurements, obtained on specimens in which the side strips are placed accurately opposite each other, will also be reported.

As specimens we used the following materials:

a) In–40at%Pb, of thickness 140 micron, which was annealed for several days at a temperature of 100°C, in order to reduce flux pinning.

b) niobium. The samples are taken out of a sheet of commercially available*) niobium, with a thickness of a 100 μ. The residual resistance at liquid helium temperatures $\rho_n \approx 4.8 \times 10^{-9}\ \Omega m$, corresponding with a residual resistance ratio $(\rho_{300}/\rho_n) \approx 27$. We studied the influence of the surface conditions by treating the sample with a piece of sandpaper and measuring the $V_{//}$ *vs* H_a curves. We compared the results with those of the original sample and with the results obtained after the surface layer had been removed again by an etching liquid. We used a mixture of one part HF, one

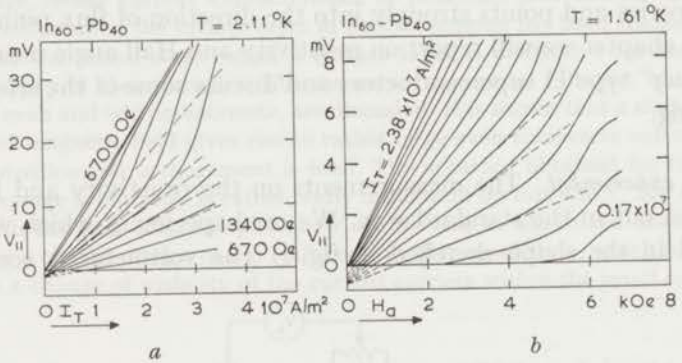

Fig. 2.

a. The longitudinal voltage as a function of the transport-current density for different values of the applied field ($H_a = n \times 670$ Oe with $n = 1 - 10$) in an In_{60}–Pb_{40} sample at $T = 2.11$°K.

b. The longitudinal voltage as a function of the applied field for $I_T = n \times 1.7 \times 10^6$ A/m² ($n = 1$–14).

part H_2SO_4, one part HNO_3 and one part H_2O. By reducing the thickness of pieces of the original Nb sheet with the etching liquid we obtained samples of 100 μ, 86 μ, 63 μ, 48 μ and 28 μ thickness. These samples, all cut out parallel to the rolling direction of the original sheet, enabled us to study the resistivity and transverse voltages as a function of the thickness, in

*) Kawecki-Billiton.

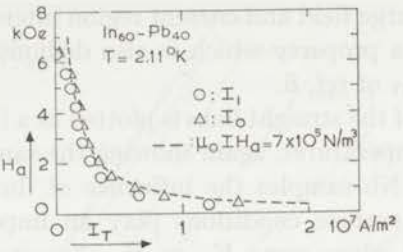

Fig. 3. The critical current densities I_0 and I_1 as a function of the applied field. The dotted curve represents a hyperbola given by $\mu_0 I \times H_a = 7 \times 10^5$ N/m³.

essentially the same material. This supplied some information about the role of the surface in these samples.

3. *The longitudinal voltages* $V_{//}$. *a*) The experimental results. In figs 2*a* and 2*b* some typical $V_{//}$ *vs* I_T and $V_{//}$ *vs* H_a characteristics are shown as obtained for the In_{60}–Pb_{40} specimens. These figures show that up to a certain critical current density $I_1(H_a)$ the voltage remains zero, due to flux pinning. In fig. 3 this critical current density I_1 is plotted as a function of the applied field H_a. The curves in fig. 2*a* show a remarkably straight character, as has earlier been noticed by Kim, Hempstead and Strnad[8]) in *e.g.* Nb_{50}–Ta_{50} and Pb_{83}–In_{17} samples. We shall comment on this point in section 3*b*. For high current densities the straight character is lost and the curves gradually tend to the characteristic of the normal state, while for the lowest current densities the curves tail off towards the zero axis. The current densities I_0, at which the extrapolated straight curves intersect the I axis, are also plotted in fig. 3, together with a hyperbola given by $\mu_0 I \cdot H_a = 7 \times 10^5$ N/m³. It is indicated in figs. 2*a* and 2*b* that the extrapolated

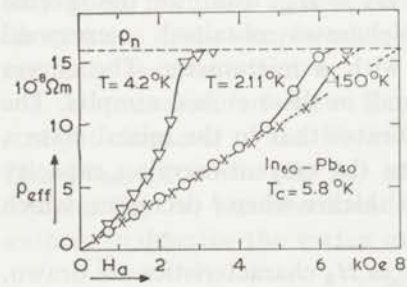

Fig. 4

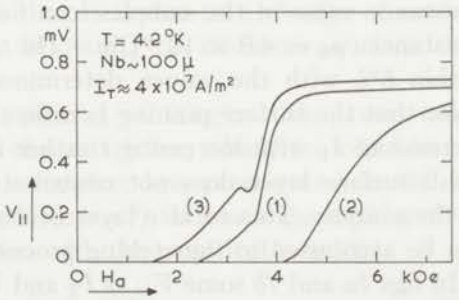

Fig. 5

Fig. 4. The slope of the straight portions of the $V_{//}$ *vs* I_T characteristics in the In_{60}–Pb_{40} samples for different temperatures.

Fig. 5. $V_{//}$ *vs* H_a characteristics for $I_T \approx 4 \times 10^7$ A/m² in a 100 μ thick Nb sample, (1) before the surface is treated with sandpaper, (2) after sandpapering and (3) after the surface layer has been removed by an etching liquid.

straight curves in a large field and current region intersect the $V_{//}$ axis quite nicely in one point, a property which is also demonstrated in the characteristics for Pb_{83}–In_{17} of ref. 8.

In fig. 4 the slope of the straight lines is plotted as a function of the applied field for different temperatures, again showing the same behaviour as found by Kim *e.a.*[8]) In the Nb samples the influence of flux pinning appears to be even larger. The surface conditions play an important role, as is demonstrated in fig. 5, where some $V_{//}$ *vs* H_a characteristics of a 100μ Nb sample are plotted for a current density $I_T = 4 \times 10^7$ A/m², before (curve 1) and after treating the surface with a piece of sandpaper (curve 2). Curve 3 shows the same characteristic after the very surface layer has been removed again with the etching liquid. It is clear from these graphs that flux motion can be completely suppressed by the surface conditions of the specimen.

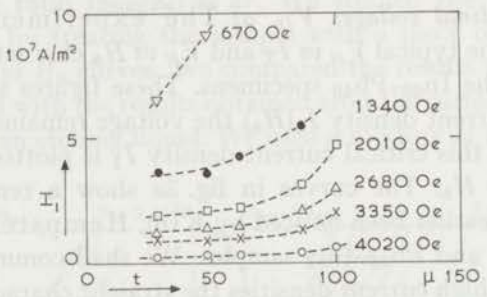

Fig. 6. The critical current density I_1 as a function of the thickness t of the Nb samples.

The influence of the surface layer on the current-carrying capacity is also demonstrated in fig. 6, where the current density I_1 at which the first measurable voltage appears is plotted as a function of the thickness t for Nb samples from essentially the same material. Curves for different values of the applied field are drawn. The thicknesses are determined from the resistance value of the samples in a field $H_a \gg H_{c_2}$, using for the specific resistance $\rho_n = 4.8 \times 10^{-9}\,\Omega$m. The thichnesses obtained correspond within 5% with the values determined with a micrometer. The curves show that the surface pinning is rather small in these etched samples. The increase of I_1 with increasing t rather indicates that in the mixed state a small surface layer does not contribute to the current-carrying capacity of the samples. This surface layer becomes thicker when t decreases, which can be attributed to the etching process.

In figs 7*a* and 7*b* some $V_{//}$ *vs* I_T and $V_{//}$ *vs* H_a characteristics are drawn, as obtained for the 63 μ and 28 μ Nb specimen respectively. These curves are typical for all our Nb samples, irrespective of the rolling direction. In fig. 7*b* we notice the well-known dip in the $V_{//}$ *vs* H_a curves in the field region just below H_{c_2}, for current densities smaller than 8×10^7 A/m². For very small current densities the curves even touch the zero-voltage axis. Although

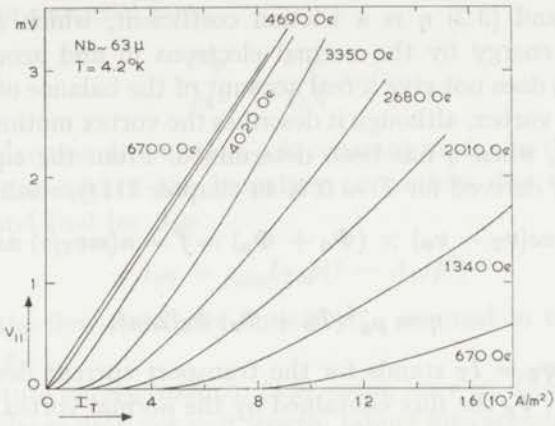

Fig. 7*a*. Typical results for $V_{//}$ *vs* I_T in the Nb samples.

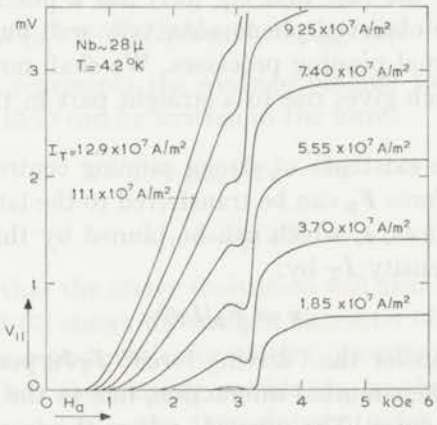

Fig. 7*b*. Typical results for $V_{//}$ *vs* H_a in the Nb samples.

it is not quite clear what mechanism is responsible for this dip in $V_{//}$, one may guess from our measurements that it is due to a change of current distribution in the sample, when just below H_{c_2}, the ineffective surface layer suddenly becomes effective.

b. Discussion of the longitudinal voltages. The remarkably straight character of the $V_{//}$ *vs* I_T characteristics, which we found in our In_{60}–Pb_{40} specimens (fig. 2*a*) and somewhat less pronounced in the Nb samples (fig. 7*a*) was also found by Kim *e.a.*[8]). It was suggested by these authors to describe the vortex motion with the empirical relation:

$$I_T \Phi_0 - F_p = \eta v_\phi \tag{3.1}$$

in which F_p is a constant force, representing the pinning of vortices, which is added to the commonly used expression for free vortex motion, when the Hall effect is neglected:

$$I_T \Phi_0 = \eta v_\phi. \tag{3.2}$$

In eqs. (3.1) and (3.2) η is a friction coefficient, which arises from the dissipation of energy by the normal electrons in and around the vortex cores. Eq. (3.2) does not give a real account of the balance of forces working on the moving vortex, although it describes the vortex motion perpendicular to the current, when η has been determined. From the equation for free vortex motion, derived for $T \approx 0°\mathrm{K}$ in chapter III[4]), reading as:

$$\tfrac{1}{2}ne(\boldsymbol{v}_\mathrm{T} - \boldsymbol{v}_\Phi) \times (\boldsymbol{\Phi}_0 + \boldsymbol{\Phi}_\mathrm{a}) = \boldsymbol{f} = n(m\boldsymbol{v}_\mathrm{T}/\tau)\,\pi a^2 \tag{3.3}$$

we find for η:

$$\eta = \rho_\mathrm{n}^{-1}(\Phi_0 + \Phi_\mathrm{a})\,\Phi_0/2\pi a^2. \tag{3.4}$$

In eq. (3.3) $ne\boldsymbol{v}_\mathrm{T} = \boldsymbol{I}_\mathrm{T}$ stands for the transport current density, $\boldsymbol{v}_\Phi$ is the vortex velocity, Φ_a the flux contained by the normal vortex cores of radius a and τ the electron-lattice collision time.

We like to stress the fact that eq. (3.1) has a purely formal character, which describes the observed phenomena very well but does not give any insight into the actual pinning processes. We shall now describe a simple pinning process which gives rise to a straight part in the $V_{//}$ *vs* I_T characteristics.

If we assume the existence of strong pinning centres in the sample, in which a maximum force F_p can be transferred to the lattice, we can express the number of vortices, ν, which can be pinned by this centre at a given transport-current density I_T by:

$$\nu = F_\mathrm{p}/I_\mathrm{T}\Phi_0. \tag{3.5}$$

These ν vortices transfer the "driving force" $I_\mathrm{T}\Phi_0$ per unit length to the pinning centre by their mutual interaction, due to the circulation currents around the vortex cores. The area A_p where the transport current flows without resistance corresponds to ν as:

$$A_\mathrm{p} = \nu\Phi_0/B = \nu/N. \tag{3.6}$$

If, for simplicity, we assume a regular square lattice (lattice constant p)

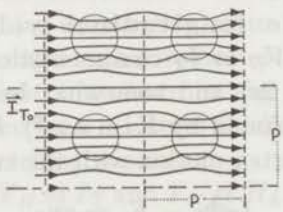

Fig. 8. Transport-current flow pattern through the pinning cells.

of these pinning centres of equal strength F_p per unit length, and, again for simplicity, we assume A_p to have the shape of a circle (fig. 8), one can immediately calculate the potential drop $-\Delta_\mathrm{p}\varphi$ across one pinning cell, from

the equation for potential flow:

$$\frac{\partial^2 \varphi}{\partial x^2} + \frac{\partial^2 \varphi}{\partial y^2} = 0 \tag{3.7}$$

with the boundary conditions that φ is constant in A_p. In the region where $A_p \ll p^2$ one can neglect the boundary corrections due to neighbouring pinning cells and find for $\Delta_p \varphi$:

$$-\Delta_p \varphi = \rho_{out} I_{To} p (1 - A_p/p^2) \tag{3.8}$$

where ρ_{out} is the flow-resistivity outside A_p, assumed to be uniform on a scale of order p.

If we substitute for A_p from eq. (3.6), using for v eq. (3.5), we obtain for the average voltage drop per unit length, taking into account the fact that, within A_p, $I_T = 2I_{To}$:

$$E_{//} = \rho_{out} I_{To}(1 - F_p/2p^2 I_{To} B) = \rho_{out} I_{To}(1 - \overline{F}_p/2I_{To} B) \tag{3.9}$$

where $\overline{F}_p \equiv F_p/p^2$ represents the average pinning force per unit volume of the sample. Eq. (3.9) can be written in the form:

$$E_{//} = \rho_{out}(I_{To} - I_0) \tag{3.10}$$

where

$$I_0 \equiv \overline{F}_p/2B. \tag{3.11}$$

It seems plausible that the above derivation will also hold for other shapes of A_p. The result (3.10) shows the straight character of the $V_{//}$ *vs* I_T characteristics for those current densities for which ρ_{out} is independent of the current. This is the case when the pinning outside A_p has been overcome by the current, so that $\rho_{out} = \rho_{eff}$, the flow resistivity for free vortex motion. Relation (3.10) then reads as:

$$E_{//} = \rho_{eff}(I_T - I_0). \tag{3.12}$$

Relation (3.12) breaks down for low current densities, when either A_p becomes of the order p^2 or ρ_{out} becomes current dependent. For high current densities eq. (3.12) is no longer valid when $2I_{To}\Phi_0 \geqslant F_p$.

From eq. (3.3) it follows that the flow resistivity in the mixed state equals:

$$\rho_{eff} = B\rho_n 2\pi a^2/(\Phi_0 + \Phi_a) \tag{3.13}$$

which shows a proportionality with B in the low-field region, where the structure of the vortex cores is independent of the magnetic induction B, so that $2\pi a^2/(\Phi_0 + \Phi_a) =$ constant. This feature is demonstrated clearly in fig. 4. In this field region, where $\rho_{eff} \sim B (B \approx \mu_0 H_a$ in these thin samples), it follows from eqs. (3.12) and (3.11) that the $V_{//}$ *vs* H_a and $V_{//}$ *vs* I_T characteristics have straight portions, which, extrapolated to $H_a = 0$ and $I_T = 0$ respectively, intersect the $V_{//}$ axis at one point (see figs. 2*a* and 2*b*). Relation

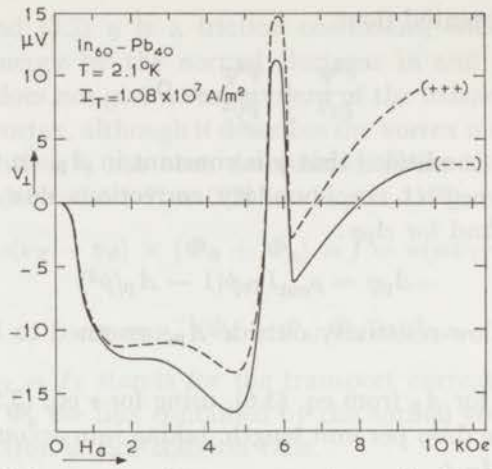

Fig. 9. Example of the measured transverse voltages in the In_{60}–Pb_{40} samples at $T = 2.1°K$. The difference between the two curves represents the uneven transverse voltage.

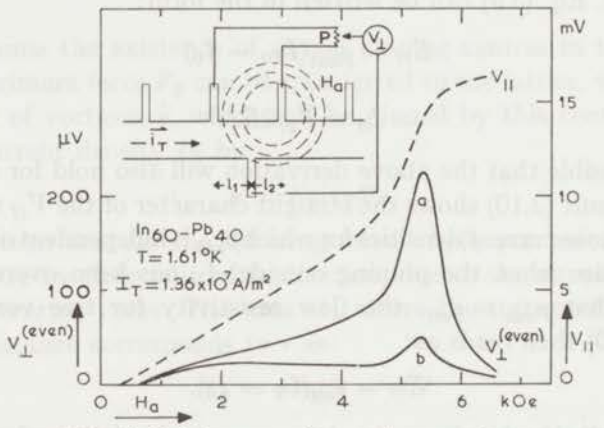

Fig. 10. Influence of the field inhomogeneity on the even transverse voltages. Curve (*a*) is measured with the sample mounted outside the axis of the Nb–Zr magnet, curve (*b*) with the sample in the centre. The insert shows the experimental situation in a nonuniform applied field.

(3.11) shows that $2\mu_0 I_0 H_a = \overline{F}_p$, which leads to a hyperbolic curve for I_0 *vs* H_a in the region where $\overline{F}_p$ is field independent. In fig. 3 we have drawn a hyperbola which nicely connects the measured I_0-values, taking for $\overline{F}_p$ the value 1.4×10^6 N/m³. This value of $\overline{F}_p$ corresponds of course with the value of $\overline{F}_p$ which can be calculated from the extrapolated $V_{//}(I_T = 0)$ value in fig. 2*a*. We have not been able to determine an accurate value for I_{To} at which $2I_{To}\Phi_0 = F_p$. If, however, we take at $T = 2.11°K$ for I_{To} the value estimated from fig. 2*a* at $I_{To} \approx 4 \times 10^7$ A/m², we find for $F_p \approx 1.6 \times 10^{-7}$ N/m and for

the average distance between the pinning centres $p = (F_p/\bar{F}_p)\frac{1}{2} \approx 3.5 \times 10^{-7}$ m $= 3500$ Å

It is clear from our results on the Nb specimens (fig. 7*a*) that in good approximation the $V_{//}$ *vs* I_T curves also satisfy eq. (3.12), though one can notice a slight curvature in these curves. This points towards a more continuous distribution of the strengths of the pinning centres throughout the samples, leading to a small current dependence of ρ_{out}.

4. *The transverse voltages,* $V_\perp$. In fig. 9 a typical example of the transverse voltage in the In_{60}–Pb_{40} samples is shown for two different orientations of field and current. One curve we have labelled with (+++), where the three + signs stand for a certain direction of current, magnetic field and recorder polarity respectively. For the (−−−) curve these three polarities are inversed. The difference between these two curves represents twice the uneven component of the transverse voltage, which reverses sign with the magnetic field and with the current (or is insensitive to both directions). The averaged curve represents the even component.

a) That the *even component* is very sensitive to the homogeneity of the applied field is demonstrated in fig. 10. Two $V_\perp$ curves measured on the same specimen are plotted together with the corresponding $V_{//}$ curve. Curve (*a*) is measured with the specimen mounted somewhat outside the axis of the Nb–Zr superconducting magnet, while curve (*b*) is measured with the centre of the specimen mounted accurately on the axis. This effect can be mainly attributed to the use of a potentiometer arrangement. In the insert of fig. 10 the experimental situation is sketched. The lines of constant magnetic field are drawn as circles. The potentiometer P is adjusted in the normal state, where the specific resistance ρ_n is independent of the magnetic field, in such a way that the even transverse voltage is zero. If in the mixed state, where ρ_{eff} is field dependent, a difference ΔH_a exists in the average field in l_1 and l_2, the potentiometer will be out of balance and an even transverse voltage will

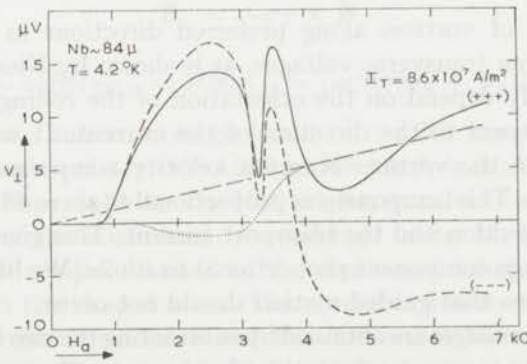

Fig. 11. The observed transverse voltages in Nb. The uneven component, obtained by subtraction of the two curves, is shown by the dotted curve.

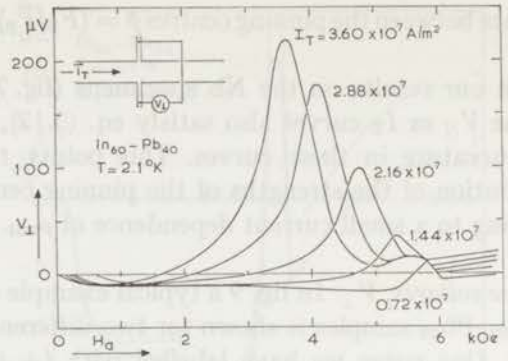

Fig. 12. Eve ntransverse voltages for different transport currents in an In_{60}–Pb_{40} sample with the transverse-voltage contacts placed accurately opposite each other.

be measured, given by:

$$V = \tfrac{1}{2} I_T \Delta\rho_{\text{eff}} l_1 \approx \tfrac{1}{2} I_T \Delta H_a (\partial\rho/\partial H_a)_{I_T} = \tfrac{1}{2}(l_1/l)\, \Delta H_a (\partial V_{//}/\partial H_a)_{I_T} \qquad (4.1)$$

The shape of the curves in fig. 10 roughly fit eq. (4.1), if we take $\Delta H_a/H_a \approx$ $\approx$ 6% for curve (*a*) and 1.5% for curve (*b*). The transverse voltage curves in the Nb specimens also demonstrate this effect (fig. 11). These curves even reflect the dip in the $V_{//}$ curves (fig. 7*a*) which shows up in the strongly varying $V_\perp$ just below H_{c_2}.

To get rid of this effect we also carried out some measurements in specimens with the transverse voltage contacts placed asccurately opposite each other. Some results are show in fig. 12. The peak in $V_\perp$ just below H_{c_2} still appears in these samples and seems to reflect $(\partial V_{//}/\partial H_a)_{I_T}$. This suggests that this effect is due to a component of the transport current in the transverse direction, which component is proportional to $(\partial\rho_{\text{eff}}/\partial H_a)$. Such a situation could arise from *e.g.* a nonuniform magnetic induction between the contacts, due to the presence of the side strips, or from a nonuniform mixed state flow resistivity in the sample caused by large scale inhomogeneities in the material.

Guided motion of vortices along preferred directions in the sample can lead to large even transverse voltages, as is shown by Niessen *e.a.*[6]). These voltages strongly depend on the orientation of the rolling direction of the sample with respect to the direction of the current. It was argued that a small fraction of the vortices obtain a velocity component parallel to the rolling direction. This component is proportional to sin α, where α is the angle between this direction and the transport current. This gives rise to an even transverse voltage component proportional to sin 2α. We have chosen $\alpha \approx 0$ in our samples so that guided motion should not occur.

b) The *uneven voltages* are obtained by subtracting the two $V_\perp$ curves, for the (+++) and the (−−−) orientation. In this way all even components are eliminated and one is left with twice the uneven $V_\perp$. (The same result could be

obtained by subtraction of the $(+++)$ and the $(+-+)$ curves, for instance, but, if any guided motion is present, this could be different in these two cases as the vortices of opposite sign follow different paths through the sample[6]). To the uneven component contribute the Hall voltage, which reverses sign with both I_T and H_a, and, if any, constant voltages, independent of the current- as well as the field-direction. Due to the rather steep slopes in the even voltages, the accuracy in the uneven voltages is rather small. A slight

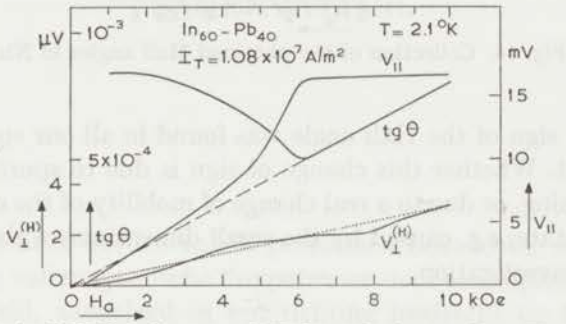

Fig. 13. The obtained Hall voltage and Hall angle for an In_{60}–Pb_{40} sample at $T = 2.0°K$ and $I_T = 2.3 \times 10^7$ A/m².

shift between the two curves along the field axis causes rather large changes in the Hall voltages obtained. In fig. 13 an example of the uneven voltage, as obtained from the curves in fig. 9, is given together with the longitudinal voltage and the Hall angle tg θ as calculated from these curves. Although the accuracy obtained is rather small it seems clear from these results that the Hall voltage follows the extrapolated straight line of the normal state. Thus an increase of the Hall angle (*i.e.* the ratio of the transverse and longitudinal electric fields) occurs on entering the mixed state, in accordance with what one can expect from eq. (33), which leads to (chapter III)[4]):

$$\boldsymbol{E}_\perp = -\boldsymbol{v}_T \times \boldsymbol{B} \tag{4.2}$$

and

$$\text{tg } \theta = v_T B / I_T \rho_{\text{eff}} = B/ne\rho_{\text{eff}} = (e\tau/m)(\Phi_0 + \Phi_a)/2\pi a^2. \tag{4.3}$$

An example of the uneven voltage found in our Nb samples, for current densities in the region of 4×10^7 A/m² to 10^8 A/m², is shown as the dotted curve in fig. 11. The results for the Hall angles, as calculated for all our Nb samples cut out of the same sheet, are collected in fig. 14, for two different temperatures. All results obtained in the above-mentioned current-density region fall within the shaded areas. The spread in the results accounts for an irregular current dependence and the differences between the various samples as well as for the irreproducibility of the results in the same sample. The Hall voltage in the normal state corresponds to 1.3–1.5 holes per atom.

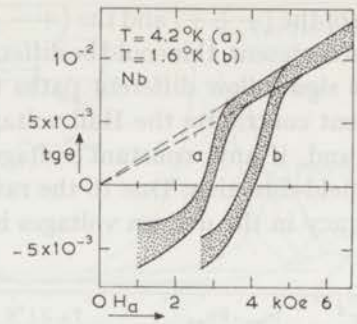

Fig. 14. Collection of the obtained Hall angles in Nb.

The change of sign of the Hall angle was found in all our specimens cut of the same sheet. Whether this change of sign is due to spurious effects *e.g.* caused by pinning, or due to a real change of mobility of the current carriers in the mixed state, *e.g.* caused by the small dimensions of the vortex cores, is still under investigation.

REFERENCES

1) Bardeen, J. and Stephen, M. J., Phys. Rev. **140** (1965) A1197.
2) Van Vijfeijken, A. G. and Niessen, A. K., Philips Res. Repts **20** (1965) 505.
3) Nozières, P. and Vinen, W. F., Phil. Mag. **14** (1966) 667.
4) Van Beelen, H., Van Braam Houckgeest, J. P., De Bruyn Ouboter, R. and Taconis, K. W., Commun. Kamerlingh Onnes Lab., Leiden No. 359*a*; Physica **36** (1967) 225.
5) Niessen, A. K. and Staas, F. A., Phys. Letters **15** (1965) 26.
Niessen, A. K., Staas, F. A. and Weysenfeld, C. H., Contributed paper to the conference on transport properties in superconductors, March 1967, Canterbury.
6) Niessen, A. K., Van Suchtelen, J., Staas, F. A. and Druyvestein, W. F., Phys. Letters **13** (1964) 293.
7) Reed, W. A., Fawcett, E. and Kim, Y. B., Phys. Rev. Letters **14** (1965) 790.
8) Kim, Y. B., Hempstead, C. F. and Strnad, A. R., Phys. Rev. **139** (1965) A1163.

SAMENVATTING

In dit proefschrift worden enkele problemen behandeld, welke optreden bij de beweging van magnetische fluxpatronen door een supergeleidend folie. Een magneetveld, aangelegd in een richting loodrecht op het oppervlak van een supergeleidend folie, zal al vanaf zeer lage veldsterkten door zo'n folie heen dringen wegens de grote ontmagnetiserings factor in deze configuratie. In een folie van type I supergeleidend materiaal zal voor velden kleiner dan het thermodynamische kritische veld dit doordringen resulteren in de zogenaamde *tussentoestand*, een patroon van normaal geleidende gebieden met een diameter in de orde van tiende millimeters, omgeven door supergeleidende gebieden. De magnetische flux dringt vrijwel uitsluitend via de normale gebieden door. Met toenemende aangelegde veldsterkte neemt de fractie normaal geleidend materiaal toe en wordt tenslotte één wanneer de kritische veldwaarde wordt overschreden.

Voor folies van type II supergeleidend materiaal treedt iets dergelijks op. Hier echter dringt de magnetische flux bij lage veldsterkten door in de vorn van vortices, resulterend in een flux patroon dat wordt aangeduid met *gemengde toestand*. Deze vortices, die ieder een flux kwant (2.07×10^{-15}Wb) bevatten, kan men zich voorstellen als een kleine cylindrische kern ($\approx$ 100 Å) van kwasi-normaal materiaal, welke naar buiten toe geleidelijk overgaat in een supergeleidend gebied waarin supergeleidende kringstromen in stand worden gehouden, zodanig dat het impulsmoment van de supergeleidende elektronenparen rondom de kern gekwantiseerd is. In een sterker wordend magneetveld neemt de dichtheid der vortices toe, onder behoud van de totale flux per vortex. Bij het overschrijden van het bovenste kritische veld wordt de normaal-toestand bereikt.

In het eerste hoofdstuk wordt de beweging van grote bundels besproken. Het feit dat deze beweging geen aanleiding geeft tot een electrisch potentiaal verschil over het folie (daar de in het normale gebied geinduceerde electrische

veldsterkte is kort gesloten door de supergeleidende omgeving) maakt het mogelijk magnetische flux in een gesloten supergeleidend circuit te "smokkelen". Een overzicht van de bestaande, op dit principe berustende, zogenaamde *fluxpompen* wordt in hoofdstuk I gegeven, tezamen met de in Leiden ontwikkelde versies. Resultaten verkregen met behulp van deze fluxpompen aan zowel draad-gewikkelde als folie-gewikkelde supergeleidende magneetspoelen worden gegeven en geanalyseerd.

Een bewegend vortex patroon kan worden verkregen zowel met behulp van een bewegende magneet als met een electrische transport stroom. In hoofdstuk II wordt een experiment besproken waarin de beweging met een bewegende magneet tot stand wordt gebracht. De hierbij optredende electrische spanningen worden geanalyseerd.

In hoofdstuk III wordt een theoretische afleiding gegeven van de bewegingsvergelijking van het vortex patroon, gedreven door een transportstroom, en van de bij deze beweging optredende spanningen. De uit deze theorie verkregen uitkomsten betreffende de te verwachten effectieve weerstand en Hall-hoek in een homogeen preparaat, waarin de vortices vrij kunnen bewegen, worden gegeven.

In hoofdstuk IV, tenslotte, vindt men een bespreking en een analyse van weerstands- en Hall-effect-metingen, verricht aan niobium- en aan In-40 at % Pb-preparaten in de gemengde toestand. De invloed van fluxpinning (het niet vrij kunnen bewegen van de vortices tengevolge van onregelmatigheden in het rooster) blijkt duidelijk uit deze metingen. Een eenvoudig model waarmee de invloed van deze fluxpinning op de resultaten te verklaren is, wordt gegeven. De voor vrije flux beweging uit de metingen af te leiden weerstand en Hall-spanningen worden vergeleken met de theoretische uitkomsten uitkomsten besproken in hoofdstuk III.

Ten einde te voldoen aan het verzoek van de Faculteit der Wiskunde en Natuurwetenschappen volgt hier een beknopt overzicht van mijn studie. Nadat ik in 1952, na het eindexamen B aan de 1e Christelijke H.B.S. te 's-Gravenhage te hebben afgelegd, mijn studie in de wiskunde en natuurwetenschappen was begonnen, legde ik in 1956 het candidaatsexamen A af. Vervolgens was ik werkzaam op het Kamerlingh Onnes Laboratorium als medewerker bij de groep onder leiding van Prof. Dr. A. F. van Itterbeek. Eerst assisteerde ik de Heer J. H. J. Herfkens bij metingen van de voortplantings-snelheid van ultra-geluid in vloeibaar helium waarna ik, in samenwerking met Dr. C. A. Velds, enige onderzoekingen verrichtte aan het magnetisch gedrag van dunne ferromagnetische lagen. In april 1959 deed ik doctoraalexamen in de experimentele natuurkunde, na hiertoe de vereiste tentamens in de theoretische natuurkunde en mechanica te hebben afgelegd.

Tot ik, in augustus 1959, in militaire dienst ging, heb ik enige maanden gewerkt in het natuurkundig laboratorium van de Rijksuniversiteit te Leuven, België, onder de leiding van Prof. Dr. A. F. van Itterbeek.

Tijdens mijn militaire diensttijd was ik als reserve officier werkzaam op het "Adviesbureau voor Wetenschappelijk Onderzoek" van de Generale Staf. In 1961 keerde ik terug op het Kamerlingh Onnes Laboratorium, nu in de werkgroep onder leiding van Prof. Dr. K. W. Taconis.

Nadat ik me eerst enige maanden heb bezig gehouden met het opzetten van een experiment met molecuulstralen heb ik de supergeleidende eigenschappen van dunne, opgedampte vanadium lagen, onderzocht. Eind 1962 vingen de experimenten aan welke beschreven zijn in dit proefschrift. Bij de ontwikkeling van de fluxpomp heb ik zeer veel steun gehad aan de actieve belangstelling van Prof. Dr. J. J. M. Beenakker. Veel medewerking ondervond ik van Mej. drs. A. J. P. T. Arnold, de Heer H. A. Sypkens en drs. J. P. van Braam Houckgeest. De hoofdstukken II en III kwamen tot stand in samenwerking met drs. J. P. van Braam Houckgeest, terwijl ik bij de metingen beschreven in hoofdstuk IV ook de medewerking ondervond van Mej. H. M. Thomas en de Heer C. Stolk.

Sinds 1957 heb ik geassisteerd op het practicum voor prae-candidaten. In oktober 1962 werd ik tot wetenschappelijk ambtenaar benoemd, in 1965 tot wetenschappelijk ambtenaar I. Sinds 1965 verzorg ik de werkcolleges behorende bij het college van Dr. J. de Nobel.

Ik spreek mijn erkentelijkheid uit voor de prettige medewerking die ik van de technische staf van het laboratorium heb ondervonden bij het tot stand komen van dit proefschrift. In het bijzonder noem ik de vindingrijkheid van de Heer E. S. Prins bij de constructie van de fluxpompen en de zorg waarmee de Heer D. W. Wijkmans de overige apparaten bouwde. Ook de bereidwilligheid waarmee de Heren L. Neuteboom en J. Turenhout de cryogene kant van de experimenten verzorgden, heb ik altijd zeer gewaardeerd.